JOURNAL OF PETROLOGY | VOLUME 48 | NUMBER 11 | PAGES 2093–2124 | 2007 | doi:10.1093/petrology/egm053

Partial Melting Experiments of Peridotite + CO_2 at 3 GPa and Genesis of Alkalic Ocean Island Basalts

RAJDEEP DASGUPTA[1,2,*], MARC M. HIRSCHMANN[1] AND NEIL D. SMITH[1]

[1]DEPARTMENT OF GEOLOGY AND GEOPHYSICS, UNIVERSITY OF MINNESOTA, 310 PILLSBURY DRIVE SE, MINNEAPOLIS, MN 55455, USA

[2]LAMONT–DOHERTY EARTH OBSERVATORY, COLUMBIA UNIVERSITY, 61 ROUTE 9W, PALISADES, NY 10964, USA

RECEIVED FEBRUARY 24, 2007; ACCEPTED AUGUST 10, 2007
ADVANCE ACCESS PUBLICATION OCTOBER 18, 2007

We document compositions of minerals and melts from 3 GPa partial melting experiments on two carbonate-bearing natural lherzolite bulk compositions (PERC: MixKLB-1 + 2·5 wt% CO_2; PERC3: MixKLB-1 + 1 wt% CO_2) and discuss the compositions of partial melts in relation to the genesis of alkalic to highly alkalic ocean island basalts (OIB). Near-solidus (PERC: 1075–1105°C; PERC3: ~1050°C) carbonatitic partial melts with <10 wt% SiO_2 and ~40 wt% CO_2 evolve continuously to carbonated silicate melts with >25 wt% SiO_2 and <25 wt% CO_2 between 1325 and 1350°C in the presence of residual olivine, orthopyroxene, clinopyroxene, and garnet. The first appearance of CO_2-bearing silicate melt at 3 GPa is ~150°C cooler than the solidus of CO_2-free peridotite. The compositions of carbonated silicate partial melts between 1350 and 1600°C vary in the range of ~28–46 wt% SiO_2, 1·6–0·5 wt% TiO_2, 12–10 wt% FeO, and 19–29 wt% MgO for PERC, and 42–48 wt% SiO_2, 1·9–0·5 wt% TiO_2, ~10·5–8·4 wt% FeO*, and ~15–26 wt% MgO for PERC3. The CaO/Al_2O_3 weight ratio of silicate melts ranges from 2·7 to 1·1 for PERC and from 1·7 to 1·0 for PERC3. The SiO_2 contents of carbonated silicate melts in equilibrium with residual peridotite diminish significantly with increasing dissolved CO_2 in the melt, whereas the CaO contents increase markedly. Equilibrium constants for Fe*–Mg exchange between carbonated silicate liquid and olivine span a range similar to those for CO_2-free liquids at 3 GPa, but diminish slightly with increasing dissolved CO_2 in the melt. The carbonated silicate partial melts of PERC3 at <20% melting and partial melts of PERC at ~15–33% melting have SiO_2 and Al_2O_3 contents, and CaO/Al_2O_3 values, similar to those of melilitic to basanitic alkali OIB, but compared with the natural lavas they are more enriched in CaO and they lack the strong enrichments in TiO_2 characteristic of highly alkalic OIB. If a primitive mantle source is assumed, the TiO_2 contents of alkalic OIB, combined with bulk peridotite/melt partition coefficients of TiO_2 determined in this study and in volatile-free studies of peridotite partial melting, can be used to estimate that melilitites, nephelinites, and basanites from oceanic islands are produced from 0–6% partial melting. The SiO_2 and CaO contents of such small-degree partial melts of peridotite with small amounts of total CO_2 can be estimated from the SiO_2–CO_2 and CaO–CO_2 correlations observed in our higher-degree partial melting experiments. These suggest that many compositional features of highly alkalic OIB may be produced by ~1–5% partial melting of a fertile peridotite source with 0·1–0·25 wt% CO_2. Owing to very deep solidi of carbonated mantle lithologies, generation of carbonated silicate melts in OIB source regions probably happens by reaction between peridotite and/or eclogite and migrating carbonatitic melts produced at greater depths.*

KEY WORDS: *alkali basalts; carbonated peridotite; experimental petrology; ocean island basalts; partial melting*

INTRODUCTION

Intra-plate basalts are key surface manifestations of dynamic processes in the Earth's mantle. Extensive trace element and isotopic studies of oceanic basalts, including those from intra-plate and plate margin settings, have established that the mantle consists of multiple reservoirs with different time-integrated compositions (e.g. Hofmann, 1997). The origin and history of these different mantle reservoirs is a matter of

*Corresponding author. Telephone: +1-845-365-8561. Fax: +1-845-365-8155. E-mail: rajdeep@ldeo.columbia.edu

considerable debate (e.g. Tackley, 2000). One key factor is that the different reservoirs may include distinct proportions of recycled crustal lithologies (e.g. Morgan & Morgan, 1999; Meibom & Anderson, 2004; Ito & Mahoney, 2005*a*, 2005*b*; Korenaga, 2005; Sobolev *et al.*, 2005) and that they might have different inventories of volatile components (Dixon *et al.*, 2002; Pineau *et al.*, 2004). These differences could give rise to different partial melting behaviours, which would influence both the possible conditions under which such sources produce basaltic lavas as well as the dynamics of melt extraction. Such variability could also influence the compositions of the resulting lavas; consequently, the petrological characteristics of oceanic island basalts (OIB) might be an important clue to the origin of mantle geochemical reservoirs. Thus, understanding the origin and history of distinct mantle reservoirs requires constraints on the partial melting behavior of a range of mantle lithologies as well as how this behavior is influenced by volatiles in intra-plate basalt source regions.

Although the lavas from large buoyancy-flux oceanic islands such as Hawaii and Iceland are commonly tholeiitic and presumably reflect large degrees of melting (Wagner & Grove, 1998; Herzberg & O'Hara, 2002; Norman *et al.*, 2002), most intra-plate basalts from smaller hotspot-related oceanic island chains are believed to represent low-degree melts (e.g. Caroff *et al.*, 1997; Holm *et al.*, 2006) and are alkalic (GEOROC database: http://georoc.mpch-mainz.gwdg.de/georoc/). The same is true for melts produced during the early and late stages of activity of Hawaiian volcanoes, such as the post-shield lavas of Mauna Kea, Hawaii (West *et al.*, 1988; Frey *et al.*, 1990), Kauai (Clague & Dalrymple, 1988; Maaløe *et al.*, 1992), the Honolulu volcanic series of Oahu (Clague & Frey, 1982), the submarine lavas of the North Arch volcanic field (Dixon *et al.*, 1997; Yang *et al.*, 2003) or the pre-shield lavas of Loihi (Garcia *et al.*, 1995; Dixon & Clague, 2001). Intra-plate seamounts with no clear relationship to hotspot tracks also produce nepheline-normative lavas (Blum *et al.*, 1996; Janney *et al.*, 2000; Kamenetsky *et al.*, 2000; Pineau *et al.*, 2004; Hirano *et al.*, 2006). Some of these lavas might originate from deep-seated mantle plumes (Morgan, 1971) and others from small-scale convective instabilities beneath the lithosphere (Raddick *et al.*, 2002).

Alkalic intra-plate oceanic lavas range in composition from slightly undersaturated alkali basalts to strongly undersaturated olivine nephelinites and olivine melilitites. Interestingly, oceanic islands with very strong isotopic signatures of crustal recycling, such as the Cook–Austral Islands, Saint Helena, Cape Verde and the Canary Islands, are characterized by highly undersaturated lavas with low silica concentrations [see reviews by Kogiso *et al.* (2003) and Dasgupta *et al.* (2006)]. Also, many such lavas carry strong indications of a role for CO_2, such as associations with carbonatites (Canaries and Cape Verde: Hoernle *et al.*, 2002), phenocrysts with CO_2-rich melt inclusions (Cook–Australs: Saal *et al.*, 1998), or xenoliths that carry evidence for carbonatite metasomatism (Canaries: Neumann *et al.*, 2002). Thus, the relationship between recycled lithologies, high concentrations of CO_2, and the petrological character of the partial melts may be a critical constraint on the origin of some flavours of OIB.

It has been known for decades that at high pressure and small melt fraction, partial melts of peridotite are broadly similar to natural alkali basalts, basanites, and nephelinites, (Green & Ringwood, 1967; Ito & Kennedy, 1967; Takahashi & Kushiro, 1983; Green & Falloon, 1998). However, in detail, experimentally derived melts of volatile-poor peridotite (Takahashi, 1986; Hirose & Kushiro, 1993; Walter, 1998) are not similar to natural alkalic lavas (Kogiso *et al.*, 2003; Dasgupta *et al.*, 2006). Also, liquids possibly parental to extremely alkalic olivine nephelinites and olivine melilitites are unlike any partial melts of volatile-poor peridotite and must derive from more exotic sources, possibly including some combination of carbonated peridotite (Hirose, 1997; Green & Falloon, 1998) and carbonated eclogite (Dasgupta *et al.*, 2006). However, many less extreme alkali basalts, basanites and nephelinites from OIB localities also have lower SiO_2 and Al_2O_3, and higher TiO_2, FeO^* and CaO at a given MgO content than experimentally derived partial melts of volatile-poor peridotite. Melts of mixtures of peridotite and basalt have similar problems (Kogiso *et al.*, 1998). Further, no reasonable fractionation scheme involving olivine or pyroxene can generate the lava compositions from parental liquids equivalent to experimental liquids generated from normal fertile peridotite or peridotite–basalt hybrids (Kogiso *et al.*, 2003; Dasgupta *et al.*, 2006). Some of these discrepancies may arise simply because there are as yet few experimental determinations of the compositions of low-degree partial melts of garnet peridotite at the appropriate pressures. Still, the aforementioned associations between alkalic OIB and indications of crustal recycling and volatile enrichment invite the hypothesis that alkalic OIB originate in part from sources that contain pyroxenites (Hirschmann *et al.*, 2003; Kogiso *et al.*, 2003) or are enriched in CO_2 (Eggler, 1978; Hémond *et al.*, 1994; Hirose, 1997; Dasgupta *et al.*, 2006).

It is well known that CO_2 reduces the silica content of mantle-derived melts (Kushiro, 1975), but experiments detailing the relationship between low-silica magmas and partial melting of natural carbonated garnet peridotite are sparse. Two types of experiments have been performed: inverse experiments, in which the saturation state of highly undersaturated magmas is examined in the presence of $CO_2 \pm H_2O$, and forward experiments, in which partial melting experiments are conducted with natural or model peridotite bulk compositions.

A large number of inverse experiments have explored liquidus phase relations of olivine melilitite in the presence of $CO_2 \pm H_2O$ at pressures ≤ 3 GPa (Brey & Green, 1975, 1976, 1977; Brey, 1978). These studies have established

that CO_2 enhances the stability of orthopyroxene on the liquidus of highly alkalic liquids at high pressure, thereby strengthening the hypothesis that low-silica liquids may be derived from partial melting of carbonated peridotite. However, none of these crystallization experiments document the major element compositions of highly alkalic liquids coexisting with mantle minerals and none achieved multiple saturation of melilititic melts with a lherzolite residue. Thus, the link between these experiments and CO_2-present partial melting of mantle lherzolite remains uncertain.

A large number of partial melting experiments have been performed with natural (Mysen & Boettcher, 1975; Wendlandt & Mysen, 1980; Olafsson & Eggler, 1983) and model carbonated peridotite compositions (Wyllie & Huang, 1976; Eggler, 1978; Dalton & Presnall, 1998*a*; Gudfinnsson & Presnall, 2005). Experiments with synthetic model compositions allowed Eggler (1974) to demonstrate that dissolved CO_2 stabilizes strongly alkalic liquids in equilibrium with peridotitic minerals. Subsequent studies in model CMAS systems confirmed that small-degree silicate partial melts of carbonated peridotite are silica-undersaturated melilititic–nephelinitic at 3–3·5 GPa (Gudfinnsson & Presnall, 2005). However, none of the studies, conducted on natural mantle compositions (Mysen & Boettcher, 1975; Wendlandt & Mysen, 1980; Olafsson & Eggler, 1983), reported major element compositions of alkalic, carbonated silicate partial melts and therefore do not place quantitative constraints on the origin of natural alkalic magmas.

To date, the sole direct high-pressure partial melting study that employed a CO_2-bearing natural peridotite and that reported compositions of highly alkalic partial melts is that of Hirose (1997). Hirose (1997) conducted partial melting studies of KLB-1 peridotite + 5% $MgCO_3$ at 3 GPa. The resulting low-silica partial melts have similarities to natural melilitites, nephelinites, and basanites. However, Dasgupta *et al.* (2006) pointed out that partial melts from the study of Hirose (1997) are too poor in TiO_2 and FeO* to be parental to many alkalic lavas. Also, whereas partial melts of natural peridotite are too low in CaO to be parental to alkalic OIB, the partial melts produced by Hirose (1997) have the interesting problem of being much richer in CaO than plausible parental melts to the natural lavas (Kogiso *et al.*, 2003; Dasgupta *et al.*, 2006). Importantly, the liquids generated by Hirose (1997) are high-degree melts (18–29 wt%), whereas natural alkalic OIB are commonly generated at low degrees of partial melting (<5%) (e.g. Tubuai, Austral Islands: Caroff *et al.*, 1997; Cape Verde: Holm *et al.*, 2006). Also, natural alkalic partial melts may be generated from sources with much less CO_2 than the 2·6 wt% employed in the experiments by Hirose (1997). For example, estimates of CO_2 in enriched mantle source regions range up to 0·1–0·4 wt% (Dixon *et al.*, 1997; Pineau *et al.*, 2004). Evaluating the influence of this excess bulk CO_2 on partial melt compositions requires experiments with variable quantities of CO_2.

In previous studies, we investigated production of carbonatitic melts at the solidus of carbonate-bearing peridotite (Dasgupta & Hirschmann, 2006, 2007*a*, 2007*b*) and the enhancement of melt fractions during the transition from lower temperature carbonatite to higher temperature carbonated silicate partial melts during upwelling beneath ridges (Dasgupta *et al.*, 2007). Here we report the compositions of carbonated silicate partial melts and of residual minerals from 3 GPa partial melting of two carbonate-bearing fertile peridotite compositions, one with 2·5 wt% CO_2 (PERC) and another with 1 wt% CO_2 (PERC3). These experiments formed the basis for our previous model on the effect of a trace quantity of CO_2 in inducing deep 'silicate melting' beneath ridges and the possible implications for the extraction of hydrogen from nominally anhydrous mantle peridotite (Dasgupta *et al.*, 2007). Carbonated silicate melting of peridotite is probable beneath ridges as well as beneath ocean islands, but OIB compositions are probably more influenced by CO_2 than are mid-ocean ridge basalts (MORB), owing to higher estimated concentrations of CO_2 in a typical OIB source mantle (e.g. Dixon *et al.*, 1997) and lower mean extents of melting. However, application of experiments to both MORB and OIB requires some extrapolation because the experiments, by necessity, must have more CO_2 than is present in either source. The chief purpose of this study is to present detailed compositional data on the minerals and partial melts generated by partial melting of carbonated garnet peridotite at 3 GPa and to use these results to investigate possible links between such melts and alkalic intraplate lavas.

EXPERIMENTAL TECHNIQUES

Starting material

The starting materials PERC and PERC3 have 2·5 wt% bulk CO_2 and 1 wt% bulk CO_2, respectively (Dasgupta & Hirschmann, 2006; Table 1). They consist of a mixture of carbonates and a fertile peridotite (MixKLB-1). The MixKLB-1 peridotite was constructed from natural olivine, opx, cpx, garnet and then dehydrated in a reducing (QFM − 1, where QFM is the quartz–fayalite–magnetite buffer) CO–CO_2 atmosphere at 1000°C for 4 h (Dasgupta & Hirschmann, 2006). The carbonate mixture was prepared with the same Ca:Mg:Fe:Na:K ratio as MixKLB-1 from natural magnesite and siderite and reagent grade $CaCO_3$, Na_2CO_3 and K_2CO_3, and then dried at 250–300°C for 4–12 h prior to mixing with the peridotite. Reaction between small amounts of Fe^{3+} in MixKLB-1 (~0·15 wt% at QFM − 1, Gudmundsson & Wood, 1995; Canil & O'Neill, 1996) with the graphite crucibles potentially added negligible (~0·02 wt%) CO_2

Table 1: Compositions (wt%) of starting materials and base peridotite

	MixKLB-1	PERC	PERC3	KLB-1 + 5% mst
SiO_2	44·54	42·29	43·63	42·26
TiO_2	0·21	0·20	0·20	0·15
Al_2O_3	3·70	3·52	3·63	3·41
Cr_2O_3	0·23	0·21	0·22	0·29
FeO*	8·08	8·07	8·08	7·70
MnO	0·14	0·13	0·14	0·11
MgO	39·30	39·26	39·27	39·65
CaO	3·52	3·52	3·52	3·27
Na_2O	0·29	0·29	0·30	0·29
K_2O	0·01	0·01	0·01	0·02
CO_2		2·51	1·02	2·61
Sum	100·01	100·01	100·01	99·75
Mg-no.	89·65	89·65	89·65	90·17
Ca-no.	5·46	5·46	5·46	5·07

*Total Fe is given as as FeO.
MixKLB-1 is the composition of the base peridotite. KLB-1 + 5% mst is the bulk composition used by Hirose (1997). Mg-number = 100 × molar Mg/(Mg + Fe); Ca-number = 100 × molar Ca/(Ca + Mg + Fe).

to PERC and PERC3 during the high-pressure experiments. The PERC and PERC3 compositions contrast with that employed in the study of Hirose (1997) (Table 1), for which 5 wt% magnesite was added to KLB-1 to make a bulk composition with 2·6 wt% CO_2. The resulting bulk composition has higher MgO, higher Mg-number [$=100 \times Mg/(Mg + Fe)$ on a molar basis], and lower Ca-number [$=100 \times Ca/(Ca + Mg + Fe)$ on a molar basis] than the compositions investigated here.

Experimental procedure

All experiments were conducted in an end-loaded piston cylinder apparatus following the procedures, calibration, and assembly described and reported in detail by Dasgupta *et al.* (2005). Homogeneous mixtures of carbonated peridotite were loaded in thick graphite crucibles with Pt outer capsules and kept in a drying oven at 120°C for a couple of hours to further ensure nominally anhydrous condition before welding the outer Pt capsule. The oxygen fugacities of the experiments were not strictly controlled, but the presence of graphite and the absence of CO_2-rich vapor requires that the charge was more reduced than the CCO (carbon-carbon monoxide/carbon dioxide) buffer (e.g. Frost & Wood, 1997) and for those experiments above 1325°C, the absence of a carbonate phase requires that it remained below the EMOG (enstatite-magnesite-olivine-graphite) buffer (e.g. Olafsson & Eggler, 1983).

Run products were polished on a soft nylon cloth using dry polycrystalline diamond powders to achieve a 0·25 μm finish. Water and other liquid lubricants were avoided during polishing to aid preservation of carbonates.

Analysis of run products

Textures and major element compositions of the resulting phases were analyzed with a JEOL JXA8900R Super Probe at the University of Minnesota. Wavelength-dispersive spectrometry (WDS) point analyses for all the phases were performed with an accelerating voltage of 15 kV. Analyses of the silicate phases were performed with fully focused beams of 10–20 nA and those of quenched melt with beam diameters varying between 5 and 100 μm and beam currents between 5 and 20 nA. Smaller melt pools (dimensions less than 20–30 μm), such as those in the interstices of residual minerals (i.e. in runs between 1300 and 1450°C), were analyzed with electron beams 5–10 μm in diameter and lower currents (5–10 nA) to avoid contamination from adjacent phases. To obtain sufficient analyses to provide representative averages of melt compositions, we analyzed as many melt pools as possible by polishing new surfaces and reanalyzing newly exposed surfaces. This process was repeated two or three times. Larger pools of segregated quenched melts were analyzed with defocused beam 25–100 μm in diameter to integrate heterogeneously quenched melt regions. Counting times for all elements were 20 s on peak and 10 s on each background for silicate minerals and carbonated silicate melts, and 10 s on peak and 5 s on backgrounds for quenched carbonate melt and carbonate minerals. Analytical standards were natural augite (Ca, Mg, Fe, and Si), omphacite (Na), garnet (Ca, Mg, Fe, Si, and Al), olivine (Fe, Mn, Mg, and Si), hornblende (Ti), K-feldspar (K), chrome spinel (Cr), and natural basalt glass (Fe, Mg, Ca, Si, and Al) for minerals and quenched silicate glass. For quenched carbonate-rich melt mattes, Ca and Mg were standardized on natural dolomite and Fe on siderite.

EXPERIMENTAL RESULTS

Experimental conditions and corresponding phase assemblages and proportions are listed in Table 2 and photomicrographs of the run products are presented in Fig. 1. Phase proportions inferred from mass-balance calculations are plotted in Fig. 2 as a function of temperature. Compositions of minerals and melts are listed in Tables 3–7 and plotted in Figs 3–5.

Phase assemblages and textures

Near-solidus phase relations for PERC have been reported by Dasgupta & Hirschmann (2006). At 3·0 GPa the subsolidus assemblage of PERC ($\leq$1075°C) comprises olivine, opx, cpx, garnet, and dolomitic solid solution. Above the solidus at 1105°C, crystalline carbonate disappears

Table 2: Summary of 3 GPa partial melting experiments with carbonate-bearing peridotite

Run no.	T (°C)	t (h)	Phases						Sum of res^2
			Ol	Opx	Cpx	Gt	Dol/cbL	sL	
PERC (peridotite + 2·5 wt% CO_2)									
A469	*1075*	*95*	*56·1 ± 0·5*	*20·1 ± 0·6*	*5·9 ± 0·4*	*12·4 ± 0·3*	*5·4 ± 0·1*	–	*0·25 ± 0·07*
A470	*1105*	*72*	+	+	+	+	+	–	
A471	1300	24	59·0 ± 0·8	17·1 ± 1·5	6·1 ± 0·9	11·8 ± 0·3	6·0 ± 0·3	–	0·05 ± 0·03
A472	1325	24	60·0 ± 1·0	17·4 ± 1·5	5·4 ± 0·9	11·0 ± 0·3	6·2 ± 0·3	–	0·03 ± 0·01
A501	1340	48	+	+	+	+	–	+	
A482	1350	24	58·5 ± 2·3	18·8 ± 4·6	4·2 ± 2·5	8·3 ± 1·4	–	10·1 ± 1·6	0·13 ± 0·18
A500	1360	48	55·5 ± 1·3	22·2 ± 2·4	–	9·2 ± 1·4	–	13·1 ± 1·4	0·69 ± 0·45
A483	1375	24	56·1 ± 1·4	23·5 ± 2·5	–	6·7 ± 1·4	–	13·7 ± 1·3	0·24 ± 0·19
A486	1400	24	57·4 ± 1·2	21·8 ± 1·8	–	5·4 ± 1·7	–	15·5 ± 1·8	0·52 ± 0·77
A488	1425	24	54·6 ± 1·8	24·1 ± 2·3	–	3·5 ± 1·5		17·7 ± 1·8	0·47 ± 0·60
A490	1450	24	54·8 ± 1·5	22·8 ± 2·0	–	–	–	22·5 ± 1·1	0·65 ± 0·70
A491	1475	24	53·1 ± 1·2	21·1 ± 2·6	–	–	–	25·8 ± 2·2	0·81 ± 0·67
A492	1500	24	54·4 ± 2·0	13·3 ± 4·0	–	–	–	32·3 ± 2·3	0·55 ± 0·51
A494	1525	24	55·9 ± 1·3	10·0 ± 2·5	–	–	–	34·1 ± 1·5	0·32 ± 0·33
A493	1550	6	57·8 ± 1·2	1·9 ± 1·8	–	–	–	40·3 ± 1·3	0·26 ± 0·22
A495	1575	6	50·2 ± 1·5	–	–	–	–	49·8 ± 1·5	0·39 ± 0·38
A496	1600	4	49·0 ± 1·1	–	–	–	–	51·0 ± 1·1	0·73 ± 0·73
PERC3 (peridotite + 1·0 wt% CO_2)									
A509	1350	24	62·4 ± 1·0	10·1 ± 1·6	13·1 ± 1·1	8·8 ± 0·5	–	5·6 ± 0·9	0·24 ± 0·06
A510	1400	25	61·7 ± 0·9	11·8 ± 1·8	12·2 ± 1·3	6·6 ± 0·7	–	7·8 ± 1·4	0·17 ± 0·08
A520	1425	25	58·1 ± 1·7	22·7 ± 3·2	–	–	–	19·2 ± 1·7	0·89 ± 0·67
A512	1450	25	59·4 ± 2·2	19·9 ± 4·5	–	–	–	20·7 ± 2·6	0·69 ± 0·81
A514	1500	23	58·4 ± 1·4	14·5 ± 2·4	–	–	–	27·1 ± 1·6	1·14 ± 0·66
A515	1550	7	59·1 ± 2·8	8·9 ± 5·4	–	–	–	32·0 ± 2·9	0·94 ± 0·71
A516	1600	4	51·8 ± 1·7	1·0 ± 2·0				47·2 ± 2·4	2·06 ± 0·71

Ol, olivine; Opx, orthopyroxene; Cpx, clinopyroxene; Gt, garnet; Dol, dolomite solid solution; cbL, carbonate-rich melt; sL, carbonated silicate melt. Modal abundance (wt%) are by mass-balance calculation using all the oxide concentrations of constituent phases; the errors are 1σ standard deviation with respect to mean for the calculated phase proportions, using uncertainties in analysed phase compositions (Tables 3–7); Sum of res^2 is the summation of squares of residuals obtained using mineral modes, phase compositions, and composition of the starting materials. Runs in italics represent experiments whose phase proportions are re-reported from Dasgupta & Hirschmann (2006). Detailed phase proportions for all the other experiments are reported here for the first time. '+' and '–' indicate presence and absence of a phase, respectively.

and a carbonatitic melt appears in equilibrium with four-phase lherzolite. At higher temperatures, quenched carbonate melts (1100–1325°C) and carbonated silicate melts (1340–1600°C) are present. No clear textural relations are observed in any runs that might indicate coexisting carbonate-rich and silicate-rich melts. The solidus for PERC3 is not bracketed experimentally at 3 GPa but it is expected to be near 1050°C based on a correlation observed between isobaric solidus temperatures of carbonated peridotite and bulk Na_2O/CO_2 ratios (Dasgupta & Hirschmann, 2007*a*). Carbonated silicate melts for PERC3 are present at 1350–1600°C. Cpx disappears between 1350 and 1360°C for PERC and between 1400 and 1425°C for PERC3, whereas garnet disappears between 1425 and 1450°C for PERC and between 1400 and 1425°C for PERC3. Opx coexists with olivine and silicate melt up to ~1550°C for PERC and up to ~1600°C for PERC3 and olivine is the liquidus phase.

Quenched carbonate melts at 1300 and 1325°C consist primarily of feathery mats of dolomite–ankerite$_{ss}$ (ss indicates solid solution) crystals and are present at triple grain junctions and along grain edges of residual olivine,

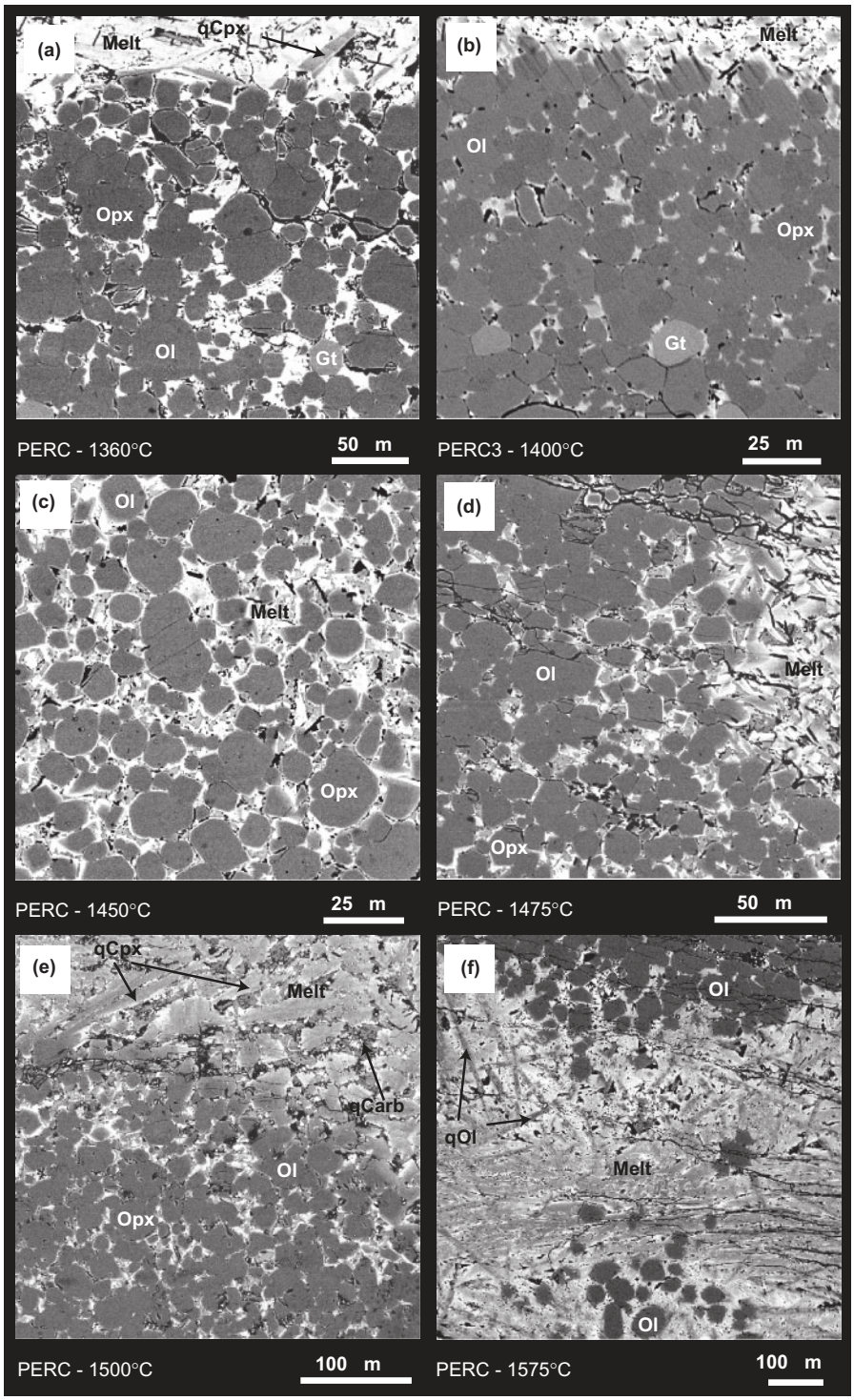

Fig. 1. Back-scattered electron images of experimental run products. Ol, olivine; Opx, orthopyroxene; Gt, garnet; Melt, carbonated silicate melts. (a) Run A500 (PERC: 1360°C, 48 h): quenched carbonate-rich silicate melt, now composed of quench cpx (qCpx) and carbonate minerals is observed along the top of the capsule; quenched melts also reside at the interstices of residual olivine, opx, and garnet. (b) Run A510 (PERC3: 1400°C, 25 h) has a pool of carbonate-rich silicate melt towards the top of the graphite capsule. (c) Run A490 (PERC: 1450°C, 24 h) shows abundant heterogeneously quenched carbonated silicate partial melt along the grain edges and at triple grain junctions of residual olivine and opx. These melts are mostly quench modified and thus avoided for estimation of equilibrium melt compositions. (d) Run A491 (PERC: 1475°C, 25 h) shows partial melts along one side of the charge with residual olivine and opx. (e) Run A492 (PERC: 1500°C, 24 h) with residual olivine, opx, and an interconnected network of quenched partial melt along the edges of the mineral grains. A large melt pool with laths of quench pyroxenes (qCpx) and interstitial quench carbonates (qCarb) is present at the top of the charge. (f) Run A495 (PERC: 1575°C, 6 h) showing a large melt pool, comprising quench cpx, quench carbonate, and blades of quench olivine (qOl), in the presence of residual olivine.

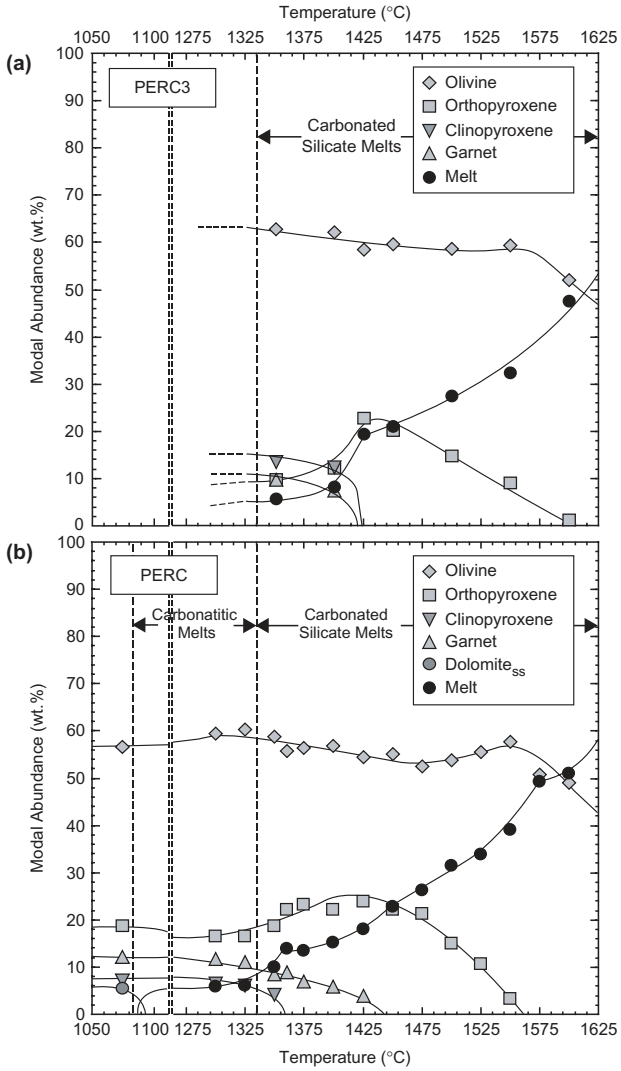

Fig. 2. Modal abundance (expressed in weight per cent) of olivine, opx, cpx, garnet, and partial melt from mass-balance calculations of PERC3 (a) and PERC (b) partial melting experiments at 3 GPa. The melts at temperatures ≤1325°C for PERC are carbonatitic and at ≥1340°C carbonate-rich silicate melts. A sharp but continuous transition from carbonatite to carbonated silicate partial melt occurs in the 3 GPa melting interval of PERC. Constraints on the solidus of PERC (1075–1105°C) and on the sub-solidus phase proportions at 1075°C are from the study of Dasgupta & Hirschmann (2006). The transition between carbonatite and carbonated silicate melts for bulk composition PERC3 is not bracketed experimentally; however, it is expected to be at a temperature similar to that observed for PERC, based on the trend of melt fraction vs temperature.

opx, cpx, and garnet. Carbonated silicate melts, at temperatures below 1550°C, consist of variable proportions of quench cpx and carbonates (Fig. 1a–e), whereas at ≥1550°C they are mats composed of quench cpx, olivine, and interstitial carbonates (Fig. 1f). Presence of glass is not observed in any runs. At relatively low temperature (≤1450°C), carbonated silicate melts remain mostly in the interstices of residual silicate minerals (Fig. 1a–d), but are also observed towards the top (Fig. 1a and b) and/or along the sides of charges (Fig. 1d).

Assessment of chemical equilibration

The experiments reported here are unreversed and the back-scattered electron images show zoning in garnet, reflecting incomplete chemical equilibration. However, an approach to chemical equilibrium can be assessed as follows. (1) For experiments in which all phases were analyzable, average sums of squared residuals ('Sum of res^2' in Table 2) are 0·41 and 0·88 for experiments with PERC and PERC3, respectively. Considering uncertainties in analyses of alkalis and estimation of CO_2 in quenched carbonated melts, these residuals are considered to be acceptable. (2) All the phases, including garnet rims, show systematic compositional shifts with increasing temperature, as described in greater detail below. For example, Al_2O_3 contents of orthopyroxenes in equilibrium with garnet increase systematically with temperature (from 1·8 to 4·3 wt% for PERC between 1075 and 1425°C and from 4·3 to 5·0 wt% for PERC3 between 1350 and 1400°C) and are consistent with the results of previous experiments at similar pressure (from 1·7 to 4·1 wt% between 1000 and 1300°C at 3 GPa: Brey *et al.*, 1990). (3) The olivine–melt K_{DFe^*-Mg} values for all runs containing carbonated silicate melts are between 0·29 and 0·38, similar to the ranges previously observed for equilibrium between olivine and carbonated silicate melt (Hirose, 1997) and olivine and basaltic liquid (Kushiro & Walter, 1998; Walter, 1998; Kushiro, 2001). Further discussion of olivine–melt K_{DFe^*-Mg} is given in the 'Discussion' section below. Observed values for K_{DFe^*-Mg} between opx and carbonated silicate melt are between 0·27 and 0·31, which are also consistent with previous determinations from peridotite with and without CO_2 (Hirose, 1997; Walter, 1998). The observed olivine–melt and opx–melt K_{DFe^*-Mg} values indicate that average compositions of quenched melt are representative of liquid compositions, and are not strongly affected by quench modifications.

Phase compositions

In this section we summarize the compositions of the six phases observed in our experiments—dolomite solid solution, partial melt, cpx, garnet, opx, and olivine—as a function of temperature across the 3 GPa melting interval of PERC and PERC3. Except where noted, partial melt compositions are reported after normalization of microprobe totals to 100% and without accounting directly for variable concentrations of CO_2.

Dolomite$_{ss}$

Subsolidus crystalline carbonate in equilibrium with PERC garnet lherzolite at 1075°C is a dolomite solid solution with

Table 3: Composition of partial melt

Run no.:	A471	A472	A482	A500	A483	A486	A488	A490	A491	A492	A494
T (°C):	1300	1325	1350	1360	1375	1400	1425	1450	1475	1500	1525
n:	7	6	11	10	10	13	12	19	18	17	16
SiO_2	5·3 (15)	7·0 (19)	28·4 (85)	32·1 (53)	32·0 (49)	34·5 (45)	35·9 (45)	37·3 (31)	40·2 (30)	41·3 (35)	42·6 (17)
TiO_2	0·91 (50)	1·21 (40)	1·61 (22)	1·44 (36)	1·42 (32)	1·25 (28)	1·15 (24)	0·95 (15)	0·9 (3)	0·82 (19)	0·75 (6)
Al_2O_3	2·2 (13)	2·7 (15)	9·8 (20)	8·8 (30)	9·2 (30)	9·5 (28)	10·2 (20)	12·3 (16)	10·8 (22)	9·9 (14)	9·40 (37)
Cr_2O_3	n.a.	n.a.	0·11 (10)	n.a.	n.a.	0·09 (5)	0·13 (9)	0·14 (5)	0·18 (6)	0·22 (4)	0·26 (5)
FeO*	7·8 (16)	7·5 (18)	11·9 (15)	11·9 (19)	11·9 (13)	11·6 (14)	11·4 (10)	10·9 (13)	11·2 (11)	11·2 (10)	10·56 (44)
MnO	0·17 (6)	0·17 (5)	0·23 (6)	0·22 (6)	0·22 (8)	0·20 (8)	0·17 (6)	0·24 (6)	0·21 (7)	0·22 (7)	0·22 (4)
MgO	13·4 (21)	14·0 (24)	19·7 (22)	19·3 (19)	19·3 (20)	19·6 (28)	19·7 (29)	21·3 (20)	22·2 (22)	24·4 (13)	24·22 (78)
CaO	25·3 (24)	25·3 (21)	25·7 (32)	24·0 (30)	23·9 (40)	21·7 (30)	20·1 (25)	15·7 (35)	13·3 (22)	11·2 (14)	11·05 (93)
Na_2O	1·08 (57)	0·98 (57)	2·64 (28)	2·3 (4)	1·87 (50)	1·6 (5)	1·4 (3)	1·1 (4)	0·9 (3)	0·83 (43)	0·83 (17)
K_2O	0·05 (2)	0·05 (3)	0·07 (5)	0·07 (5)	0·07 (4)	0·05 (3)	0·03 (3)	0·10 (7)	0·09 (9)	0·07 (6)	0·10 (2)
Sum	56·18	58·86	100·00	100·00	100·00	100·00	100·00	100·00	100·00	100·00	100·00
CO_2 (by diff.)			24·9 (43)	20·3 (30)	19·1 (30)	15·4 (21)	13·3 (20)	10·5 (20)	9·6 (25)	8·8 (25)	7·1 (27)
CO_2 (mass bal.)	—	—	24·9 (36)	18·6 (26)	18·2 (23)	17·0 (21)	14·6 (17)	11·1 (19)	9·5 (19)	7·9 (21)	7·5 (21)
Mg-no.	75·29	76·80	74·72	74·27	74·26	75·13	75·54	77·62	77·90	79·54	80·34

Run no.:	A493	A495	A496	A509[1]	A510[1]	A520[1]	A512[1]	A514[1]	A515[1]	A516[1]
T (°C):	1550	1575	1600	1350	1400	1425	1450	1500	1550	1600
n:	23	33	40	9	10	12	19	22	38	41
SiO_2	45·2 (15)	45·7 (12)	45·62 (84)	42·4 (38)	43·8 (35)	43·4 (31)	44·0 (44)	45·9 (40)	47·5 (33)	48·2 (30)
TiO_2	0·51 (8)	0·48 (6)	0·49 (4)	1·86 (36)	1·36 (29)	1·09 (22)	1·06 (17)	0·98 (15)	0·66 (13)	0·51 (13)
Al_2O_3	8·85 (53)	7·29 (27)	6·83 (26)	10·0 (21)	11·0 (19)	12·5 (15)	12·7 (16)	10·5 (13)	8·8 (10)	7·55 (67)
Cr_2O_3	0·32 (5)	0·38 (9)	0·34 (5)	0·16 (6)	0·16 (9)	0·36 (35)	0·34 (36)	0·31 (30)	0·3 (3)	0·29 (6)
FeO*	10·54 (32)	10·15 (29)	9·77 (39)	10·4 (14)	10·7 (18)	9·9 (16)	9·5 (19)	9·4 (18)	9·0 (13)	8·38 (63)
MnO	0·20 (8)	0·21 (3)	0·21 (4)	0·17 (9)	0·13 (9)	0·20 (5)	0·20 (6)	0·18 (6)	0·22 (3)	0·18 (4)
MgO	25·0 (11)	28·1 (13)	28·84 (84)	15·3 (16)	16·3 (18)	16·1 (23)	16·0 (23)	18·9 (21)	21·9 (17)	26·5 (17)
CaO	8·70 (52)	7·12 (60)	7·25 (45)	17·0 (22)	14·3 (18)	15·1 (27)	15·0 (30)	12·7 (21)	10·8 (16)	7·8 (16)
Na_2O	0·62 (21)	0·57 (6)	0·61 (7)	2·73 (53)	2·11 (46)	1·28 (33)	1·19 (34)	1·1 (3)	0·81 (27)	0·70 (25)
K_2O	0·05 (4)	0·04 (2)	0·03 (2)	0·05 (4)	0·11 (7)	0·02 (3)	0·06 (3)	0·06 (3)	0·05 (3)	0·04 (2)
Sum	100·00	100·00	100·00	100·00	100·00	100·00	100·00	100·00	100·00	100·00
CO_2 (by diff.)	5·6 (15)	5·2 (19)	4·2 (12)	19·4 (37)	12·7 (30)	8·0 (40)	6·0 (40)	5·0 (40)	3·5 (22)	2·4 (22)
CO_2 (mass bal.)	6·0 (13)	5·1 (13)	5·0 (10)	15·8 (35)	13·1 (29)	5·1 (36)	4·8 (37)	3·6 (25)	3·1 (20)	2·1 (20)
Mg-no.	80·87	83·14	84·02	72·41	73·13	74·39	75·02	78·08	81·29	84·91

[1]Runs with PERC3.
*Total Fe is given as as FeO.
Errors in parentheses are 1σ of the mean, reported as least units cited; for example, 5·3 (15) should be read as 5·3 ± 1·5 wt%. *n*, number of analyses averaged; n.a., not analysed. All the analyses are reported on a CO_2-free basis, except for runs A471 and A472, where analytical concentrations are reported for carbonatite.

molar Ca/(Ca + Mg) of 0·53, Mg-number of 91·9 and FeO* of 3·0 ± 0·5 wt%.

Partial melt

We have no direct method of analyzing the concentration of CO_2 in partial melts, as they did not quench to a glass. The CO_2 in the melts may be estimated by difference between 100% and the observed microprobe totals. Alternatively, it may be estimated for those experiments where solid carbonate is absent by assuming that all CO_2 present in the charge resides in the melt and from the melt fraction determined by mass balance (see below).

Table 4: Composition of clinopyroxene

Run no.:	A469	A470	A471	A472	A501	A482	A509[1]	A510[1]
T (°C):	1075	1100	1300	1325	1340	1350	1350	1400
n:	7	6	12	13	9	11	10	11
SiO_2	53·15 (48)	54·15 (44)	53·98 (68)	53·93 (79)	54·13 (35)	54·13 (59)	53·35 (31)	53·45 (27)
TiO_2	0·55 (11)	0·56 (13)	0·20 (11)	0·14 (4)	0·15 (5)	0·15 (7)	0·19 (4)	0·15 (3)
Al_2O_3	4·79 (58)	3·65 (67)	3·95 (58)	4·19 (9)	3·98 (10)	3·68 (20)	4·75 (7)	5·36 (14)
Cr_2O_3	0·37 (5)	0·39 (8)	0·33 (5)	0·39 (3)	0·35 (4)	0·35 (6)	0·48 (4)	0·55 (6)
FeO*	3·34 (21)	3·42 (10)	3·87 (21)	3·92 (9)	3·88 (15)	3·85 (18)	3·94 (9)	4·34 (25)
MnO	0·05 (5)	0·11 (4)	0·12 (6)	0·10 (4)	0·12 (7)	0·12 (5)	n.a.	n.a.
MgO	17·41 (73)	17·93 (65)	19·56 (73)	20·29 (25)	19·89 (42)	19·87 (49)	19·79 (33)	20·79 (30)
CaO	18·98 (55)	18·43 (32)	17·29 (55)	16·74 (18)	17·27 (21)	17·27 (41)	16·25 (23)	14·76 (44)
Na_2O	1·37 (5)	1·07 (7)	0·83 (5)	0·74 (6)	0·70 (5)	0·75 (3)	0·73 (5)	0·63 (3)
K_2O	0·01 (2)	0·03 (1)	0·02 (2)	0·02 (2)	0·02 (1)	0·02 (2)	0·03 (2)	0·02 (1)
Sum	100·01	99·74	100·14	100·47	100·49	100·19	99·52	100·05
Mg-no.	90·29	90·34	90·02	90·23	90·15	90·21	89·95	89·52

[1]Runs with PERC3.
*Total Fe given as FeO.
n.a., not analyzed.

Table 5: Composition of garnet

Run no.:	A469	A470	A471	A472	A501	A482	A500	A483	A486	A488	A509[1]	A510[1]
T (°C):	1075	1100	1300	1325	1340	1350	1360	1375	1400	1425	1350	1400
n:	3	4	7	8	9	8	10	9	10	13	10	10
SiO_2	42·28 (41)	42·68 (39)	43·36 (26)	42·74 (28)	42·27 (31)	42·67 (35)	42·81 (65)	42·93 (43)	43·27 (38)	42·62 (30)	41·80 (42)	42·16 (10)
TiO_2	0·12 (5)	0·30 (3)	0·27 (3)	0·29 (5)	0·25 (5)	0·25 (3)	0·24 (2)	0·18 (3)	0·12 (4)	0·11 (4)	0·22 (3)	0·17 (7)
Al_2O_3	21·42 (11)	21·61 (21)	22·09 (17)	22·74 (14)	22·80 (11)	22·72 (21)	22·80 (61)	22·83 (41)	22·46 (24)	23·15 (57)	24·28 (22)	23·79 (20)
Cr_2O_3	1·27 (2)	1·04 (3)	0·91 (4)	1·03 (8)	1·07 (10)	1·10 (8)	1·10 (12)	1·18 (9)	1·28 (4)	1·40 (13)	1·12 (7)	1·25 (7)
FeO*	11·13 (55)	8·85 (37)	6·63 (14)	6·57 (9)	6·62 (8)	6·55 (13)	6·51 (17)	6·23 (12)	6·14 (18)	6·12 (19)	6·76 (25)	6·44 (9)
MnO	0·36 (5)	0·34 (6)	0·25 (3)	0·24 (2)	0·28 (5)	0·27 (4)	0·27 (6)	0·22 (4)	0·25 (3)	0·20 (3)	n.a.	n.a.
MgO	18·61 (42)	20·37 (30)	21·23 (13)	20·89 (23)	20·85 (22)	21·08 (38)	21·08 (36)	21·31 (34)	21·41 (27)	21·55 (70)	20·68 (25)	20·94 (39)
CaO	4·88 (17)	4·56 (13)	5·32 (12)	5·47 (18)	5·61 (15)	5·34 (12)	5·34 (25)	5·26 (21)	5·02 (23)	4·73 (22)	5·40 (10)	5·23 (31)
Na_2O	0·03 (3)	0·07 (4)	0·09 (4)	0·07 (1)	0·03 (2)	0·01 (1)	0·01 (3)	0·07 (4)	0·09 (3)	0·03 (2)	0·01 (1)	0·00 (1)
K_2O	0·03 (2)	0·01 (2)	0·02 (1)	0·03 (2)	0·02 (2)	0·02 (2)	0·02 (1)	0·02 (2)	0·03 (2)	0·01 (2)	0·02 (2)	0·02 (1)
Sum	100·13	99·83	100·17	100·13	99·79	99·94	100·12	100·63	100·07	99·93	100·29	100·00
Mg-no.	74·88	80·4	85·10	85·01	84·89	85·16	85·23	86·13	86·14	86·25	84·50	85·28

[1]Runs with PERC3.
*Total Fe given as FeO.

Both estimates are given in Table 3 and, as shown in Fig. 6, these independent methods are substantially in agreement, lending confidence to their accuracy. Major element oxide concentrations of experimental partial melts are reported in Table 3 and plotted as a function of temperature in Fig. 3.

At 3 GPa, carbonatitic partial melt from PERC, the bulk composition with 2·5 wt% CO_2, at 1300–1325°C is broadly calcio-dolomitic with molar Ca/(Ca + Mg) of 0·57–0·58 and Mg-number of 75–77. Slight increases in SiO_2, TiO_2, and Al_2O_3 are apparent from 1300 to 1325°C.

Table 6: Composition of orthopyroxene

Run no.:	A469	A470	A471	A472	A501	A482	A500	A483	A486	A488	A490
T (°C):	1075	1105	1300	1325	1340	1350	1360	1375	1400	1425	1450
n:	7	7	12	13	17	16	12	11	14	15	14
SiO_2	56·14 (57)	56·06 (23)	56·02 (47)	56·24 (37)	55·73 (40)	55·50 (14)	55·73 (27)	55·73 (29)	55·41 (19)	55·57 (60)	55·09 (11)
TiO_2	0·13 (6)	0·25 (6)	0·08 (2)	0·07 (4)	0·08 (3)	0·07 (4)	0·01 (2)	0·07 (2)	0·06 (3)	0·06 (3)	0·05 (3)
Al_2O_3	1·80 (76)	2·38 (34)	3·22 (20)	3·29 (17)	3·68 (22)	3·71 (36)	3·67 (3)	3·87 (5)	3·95 (11)	4·27 (41)	4·40 (44)
Cr_2O_3	0·24 (5)	0·19 (7)	0·21 (3)	0·21 (4)	0·28 (9)	0·28 (5)	0·30 (6)	0·31 (6)	0·35 (3)	0·37 (7)	0·39 (4)
FeO*	6·02 (27)	6·20 (8)	5·87 (16)	5·77 (13)	5·64 (14)	5·59 (4)	5·54 (16)	5·51 (17)	5·42 (24)	5·36 (9)	5·09 (12)
MnO	0·14 (4)	0·12 (3)	0·12 (5)	0·13 (3)	0·15 (3)	0·14 (2)	0·13 (4)	0·14 (3)	0·12 (3)	0·14 (3)	0·15 (5)
MgO	34·79 (67)	33·90 (58)	32·50 (30)	32·51 (24)	32·44 (22)	32·56 (16)	32·64 (70)	32·60 (69)	32·91 (22)	33·08 (50)	33·26 (50)
CaO	0·66 (26)	0·98 (17)	1·60 (6)	1·63 (9)	1·68 (10)	1·77 (14)	1·83 (19)	1·97 (8)	1·88 (9)	1·51 (11)	1·44 (10)
Na_2O	0·10 (4)	0·13 (3)	0·16 (3)	0·11 (3)	0·12 (4)	0·13 (2)	0·06 (5)	0·22 (5)	0·14 (3)	0·11 (1)	0·11 (3)
K_2O	0·01 (2)	0·03 (2)	0·02 (3)	0·02 (2)	0·03 (2)	0·03 (2)	0·01 (3)	0·01 (1)	0·00 (1)	0·03 (2)	0·01 (1)
Sum	100·04	100·24	99·80	99·99	99·82	99·78	99·31	100·40	100·25	100·44	99·99
Mg-no.	91·15	90·69	90·80	90·94	91·11	91·03	91·31	91·34	91·54	91·66	91·77

Run no.:	A491	A492	A494	A493	A509[1]	A510[1]	A520[1]	A512[1]	A514[1]	A515[1]	A516[1]
T (°C):	1475	1500	1525	1550	1350	1400	1425	1450	1500	1550	1600
n:	10	11									
SiO_2	54·73 (66)	55·78 (41)	55·85 (46)	55·87 (47)	55·13 (26)	54·57 (32)	55·15 (4)	55·29 (19)	55·83 (24)	56·02 (19)	56·96 (13)
TiO_2	0·05 (3)	0·04 (2)	0·04 (3)	0·02 (0)	0·10 (4)	0·09 (0)	0·07 (4)	0·09 (2)	0·07 (2)	0·02 (2)	0·03 (1)
Al_2O_3	4·30 (53)	3·87 (22)	3·69 (28)	3·63 (57)	4·26 (18)	4·95 (16)	4·11 (12)	3·87 (28)	3·70 (21)	2·96 (12)	2·00 (13)
Cr_2O_3	0·42 (5)	0·42 (5)	0·45 (5)	0·47 (14)	0·30 (6)	0·37 (4)	0·39 (6)	0·40 (6)	0·41 (7)	0·43 (5)	0·45 (3)
FeO*	5·05 (10)	4·72 (9)	4·62 (14)	4·20 (17)	6·06 (9)	6·00 (5)	5·66 (10)	5·35 (13)	4·99 (16)	4·94 (16)	4·32 (14)
MnO	0·12 (2)	0·12 (4)	0·12 (2)	0·15 (2)	n.a.	n.a.	0·12 (1)	0·14 (4)	0·15 (3)	0·10 (1)	0·11 (1)
MgO	33·62 (72)	33·75 (14)	33·87 (42)	34·10 (59)	32·32 (26)	32·36 (12)	32·50 (47)	32·56 (5)	33·07 (25)	33·96 (39)	34·87 (29)
CaO	1·36 (9)	1·25 (7)	1·19 (8)	1·14 (7)	1·69 (6)	1·84 (4)	2·14 (10)	2·22 (8)	1·78 (15)	1·49 (7)	1·23 (6)
Na_2O	0·11 (2)	0·10 (2)	0·08 (2)	0·09 (1)	0·11 (3)	0·11 (0)	0·12 (5)	0·14 (1)	0·10 (1)	0·08 (2)	0·04 (1)
K_2O	0·00 (1)	0·02 (1)	0·02 (2)	0·02 (2)	0·02 (2)	0·01 (1)	0·02 (2)	0·04 (1)	0·02 (1)	0·01 (1)	0·05 (1)
Sum	99·73	100·07	99·94	99·68	100·00	100·31	100·29	100·89	100·12	100·03	100·06
Mg-no.	92·27	92·73	92·89	93·53	90·48	90·57	91·10	91·57	92·20	92·45	93·50

[1]Runs with PERC3.
*Total Fe given as FeO.

Compositions of near-solidus carbonatitic partial melts could not be obtained for run A470 (1100°C: PERC) because interstitial melt pools are very small (<2–3 μm). A sharp transition from carbonatitic melts (<10 wt% SiO_2, >40 wt% CO_2) to carbonate-rich silicate melts (>25 wt% SiO_2, <25 wt% CO_2) is observed between 1325 and 1340°C for bulk composition PERC (Dasgupta *et al.*, 2007; Fig. 2). PERC partial melts become progressively more silica-rich with increasing temperature, changing from melilititic to nephelinitic to basanitic (LeBas, 1989) from 1350 to 1600°C. Low microprobe (~75–96 wt%) totals in replicate analyses of quenched silicate melts indicate that PERC-derived partial silicate melts contain *c.* 25–4·0 wt% dissolved CO_2. SiO_2 and MgO increase steadily from 28·4 ± 8·5 and 19·7 ± 2·2 wt% at 1350°C to 45·62 ± 0·84 and 28·84 ± 0·84 wt% at 1600°C respectively, whereas TiO_2 (from 1·61 ± 0·22 to 0·49 ± 0·04 wt%), FeO* (from 11·9 ± 1·9 to 9·77 ± 0·39 wt%), CaO (25·7 ± 3·2 to 7·25 ± 0·45 wt%), and Na_2O (from 2·64 ± 0·28 to 0·61 ± 0·07 wt%) decrease over the same temperature interval. The alumina content of the carbonated silicate partial melt increases from 9·8 ± 3·0 at 1350°C to 12·3 ± 1·6 at 1450°C, but diminishes to 6·83 ± 0·26 wt% at 1600°C, after disappearance of garnet from the residue at 1425–1450°C.

Table 7: Composition of olivine

Run no.:	A469	A470	A471	A472	A501	A482	A500	A483	A486	A488	A490	A491
T (°C):	1075	1105	1300	1325	1340	1350	1360	1375	1400	1425	1450	1475
n:	7	6	10	11	15	15	12	13	16	10	12	17
SiO_2	40·28	40·91 (12)	40·64 (29)	40·74 (20)	41·07 (31)	40·81 (27)	40·62 (31)	40·72 (90)	40·57 (20)	40·16 (24)	41·03 (31)	40·24 (43)
TiO_2	0·04	0·04 (3)	0·02 (3)	0·01 (1)	0·01 (2)	0·01 (1)	0·00 (0)	0·00 (0)	0·01 (3)	0·01 (0)	0·01 (1)	0·01 (2)
Al_2O_3	0·07	0·06 (6)	0·06 (2)	0·08 (2)	0·08 (2)	0·05 (4)	0·10 (3)	0·16 (20)	0·08 (2)	0·09 (1)	0·09 (4)	0·10 (2)
Cr_2O_3	0·02	0·03 (3)	0·02 (3)	0·06 (2)	0·06 (2)	0·02 (1)	0·02 (2)	0·02 (3)	0·05 (4)	0·03 (2)	0·05 (4)	0·08 (4)
FeO*	9·91	9·94 (10)	9·47 (13)	9·44 (9)	9·14 (10)	9·20 (23)	9·02 (16)	9·02 (16)	8·83 (20)	8·87 (23)	8·07 (19)	8·00 (8)
MnO	0·12	0·12 (5)	0·16 (5)	0·13 (4)	0·10 (6)	0·10 (4)	0·15 (5)	0·15 (5)	0·13 (4)	0·13 (3)	0·13 (4)	0·12 (4)
MgO	49·51	48·92 (27)	49·43 (35)	48·87 (27)	49·71 (40)	49·56 (60)	49·84 (33)	49·94 (69)	49·67 (49)	50·40 (45)	50·11 (37)	51·14 (52)
CaO	0·13	0·08 (2)	0·13 (3)	0·18 (2)	0·16 (3)	0·13 (4)	0·20 (3)	0·20 (8)	0·19 (2)	0·19 (2)	0·18 (3)	0·17 (3)
Na_2O	0·01	0·02 (2)	0·02 (3)	0·03 (1)	0·02 (2)	0·02 (2)	0·07 (2)	0·07 (3)	0·05 (3)	0·03 (3)	0·02 (2)	0·02 (2)
K_2O	0·02	0·02 (1)	0·02 (2)	0·02 (1)	0·03 (2)	0·03 (1)	0·02 (2)	0·02 (1)	0·01 (2)	0·03 (2)	0·02 (2)	0·02 (2)
Sum	100·10	100·13	99·97	99·57	100·37	99·91	100·05	100·31	99·61	99·94	99·91	99·90
Mg-no.	89·91	89·76	90·29	90·22	90·65	90·57	90·78	90·80	90·93	91·02	91·14	91·93

Run no.:	A492	A494	A493	A495	A496	A509[1]	A510[1]	A520[1]	A512[1]	A514[1]	A515[1]	A516[1]
T (°C):	1500	1525	1550	1575	1600	1350	1400	1425	1450	1500	1550	1600
n:	18	18	19	16	14	13	12	14	19	15	18	20
SiO_2	41·23 (32)	41·33 (31)	41·19 (41)	41·56 (19)	41·62 (24)	41·02 (41)	40·45 (30)	40·60 (15)	41·04 (45)	41·04 (26)	41·24 (29)	41·38 (36)
TiO_2	0·00 (1)	0·01 (1)	0·01 (2)	0·01 (2)	0·01 (1)	0·01 (2)	0·02 (3)	0·01 (1)	0·00 (1)	0·01 (1)	0·01 (1)	0·01 (2)
Al_2O_3	0·12 (3)	0·13 (2)	0·11 (4)	0·08 (2)	0·10 (2)	0·09 (4)	0·07 (2)	0·10 (3)	0·12 (2)	0·13 (3)	0·12 (2)	0·10 (3)
Cr_2O_3	0·06 (3)	0·08 (3)	0·08 (3)	0·11 (3)	0·11 (3)	0·05 (3)	0·04 (2)	0·08 (4)	0·11 (3)	0·10 (6)	0·10 (3)	0·12 (3)
FeO*	7·45 (21)	7·33 (9)	7·18 (15)	6·47 (14)	6·46 (9)	10·02 (16)	9·77 (8)	9·03 (13)	8·87 (26)	8·02 (16)	7·28 (13)	6·28 (19)
MnO	0·14 (4)	0·13 (3)	0·13 (5)	0·09 (4)	0·12 (3)	n.a.	n.a.	0·13 (3)	0·12 (3)	0·12 (4)	0·12 (3)	0·10 (4)
MgO	50·75 (26)	50·65 (24)	50·70 (32)	51·76 (20)	51·21 (27)	49·63 (43)	49·39 (44)	49·81 (13)	49·94 (34)	50·68 (39)	50·92 (75)	51·87 (51)
CaO	0·18 (4)	0·16 (3)	0·17 (3)	0·13 (2)	0·12 (3)	0·16 (5)	0·18 (4)	0·24 (5)	0·22 (4)	0·23 (5)	0·23 (1)	0·18 (4)
Na_2O	0·02 (1)	0·02 (2)	0·01 (2)	0·01 (1)	0·01 (1)	0·01 (1)	0·01 (1)	0·03 (2)	0·02 (2)	0·01 (1)	0·02 (1)	0·02 (2)
K_2O	0·01 (1)	0·02 (1)	0·02 (2)	0·02 (1)	0·02 (1)	0·01 (1)	0·01 (2)	0·01 (1)	0·01 (1)	0·03 (1)	0·01 (1)	0·03 (2)
Sum	99·96	99·85	99·61	99·92	99·78	101·01	99·95	100·03	100·44	100·38	100·05	100·08
Mg-no.	92·39	92·49	92·64	93·45	93·39	89·83	90·01	90·77	90·96	91·84	92·58	93·64

[1]Runs with PERC3.
*Total Fe given as FeO.

Carbonated silicate partial melts of PERC3, the bulk composition with 1 wt% CO_2, vary from nephelinitic at low temperature to basanitic at higher temperature and show temperature vs oxide concentration trends similar to melts from PERC, with the chief differences being higher SiO_2, TiO_2 and Na_2O, and lower MgO, FeO* and CO_2, at any given temperature. Also, at relatively low temperatures (1350–1450°C), partial melts are distinctly less calcic than those of PERC.

Clinopyroxene

Cpx compositions show little variation across the melting interval of PERC and PERC3. Mg-numbers are nearly constant at ~90 (Table 4). Na_2O concentration drops from $1{\cdot}37 \pm 0{\cdot}05$ to $1{\cdot}07 \pm 0{\cdot}07$ wt% across the solidus with the formation of carbonatitic melt and drops further to ~0·7 wt% with enhanced melting and the formation of carbonated silicate melts.

Garnet

Garnet compositions are given in Table 5 and plotted as a function of temperature across the carbonated silicate-melting interval in Fig. 4. Systematic and steady decreases in TiO_2 and FeO* and increases in Cr_2O_3 are observed for both PERC and PERC3 bulk compositions across the melting interval. MgO contents vary between ~20·5 and

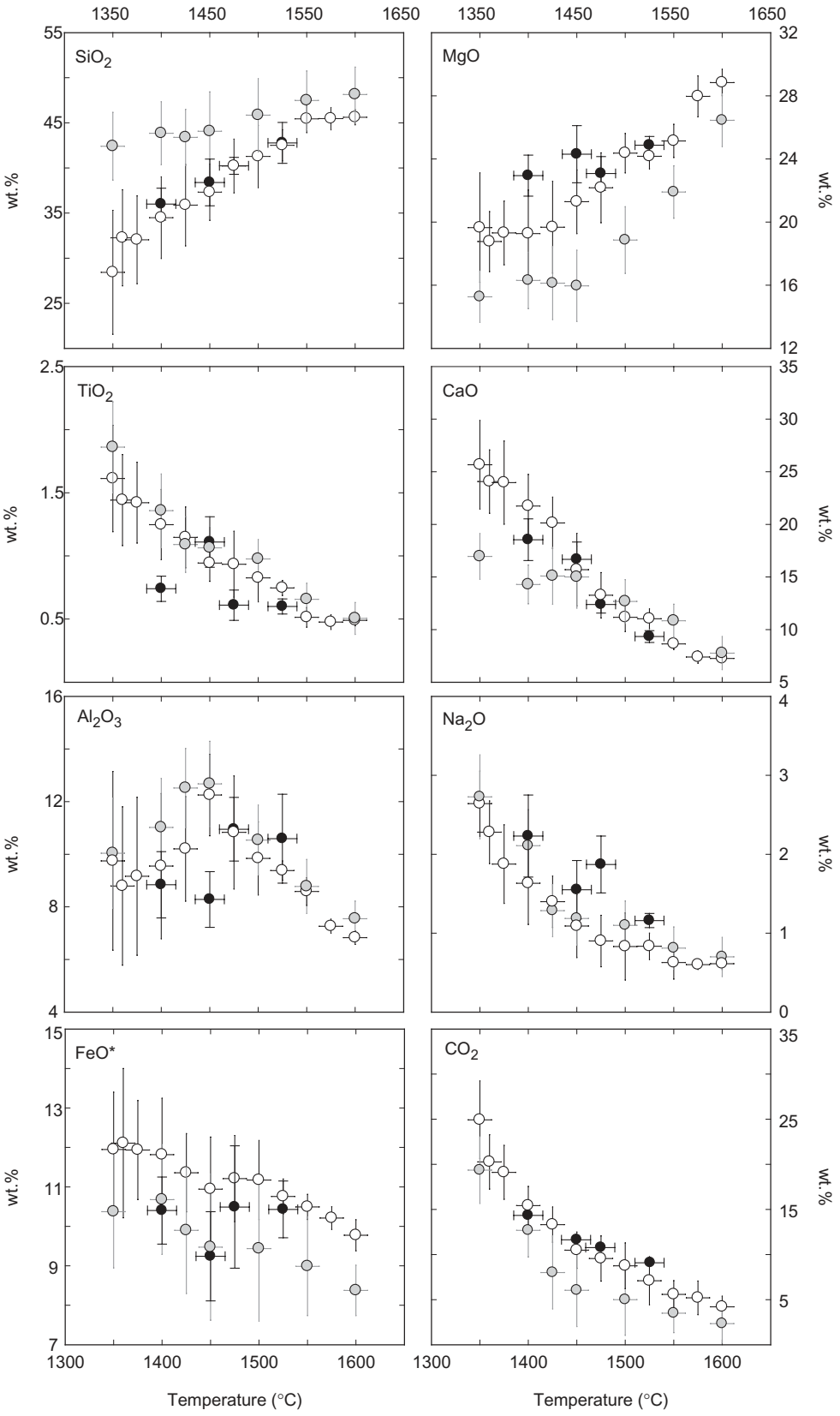

Fig. 3. Composition of carbonate-bearing silicate partial melts from PERC (white circles) and PERC3 (grey circles) carbonated peridotite partial melting experiments at 3 GPa. Concentrations of SiO_2, TiO_2, Al_2O_3, FeO*, MgO, CaO, and Na_2O are calculated on a volatile-free basis and that of CO_2 is derived by the difference between 100% and the average total from replicate electron microprobe analyses. Also included for comparison are carbonated silicate partial melt compositions from the study of Hirose (1997) (•). Concentrations of CO_2 in the experiments of Hirose (1997) are estimated from bulk CO_2 in the experiments and estimates of melt fractions. The latter are estimated from mass balance for experiments at 1400 and 1525°C, where mineral phases are reported, and by linear interpolation of these melt fractions vs temperature for experiments at 1450 and 1475°C. Error bars in temperature are ±12°C and ±15°C for this study and Hirose (1997) respectively and for composition $\pm 1\sigma$ (wt%) for both studies.

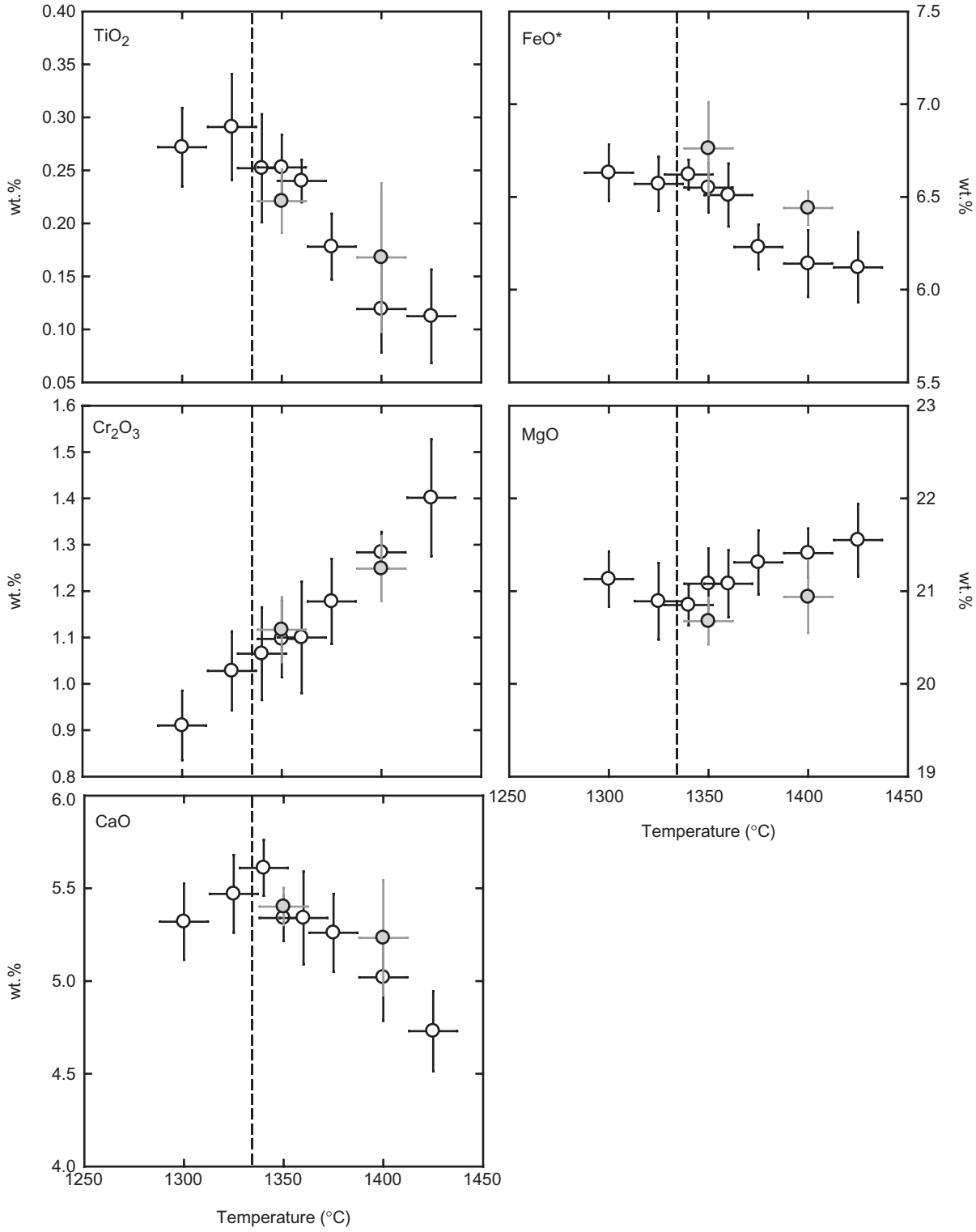

Fig. 4. Compositions of garnet from 3 GPa PERC and PERC3 carbonated peridotite partial melting experiments. The dashed vertical line marks the temperature of initiation of 'silicate melting' based on experiments with PERC. The relatively small variations in CaO and TiO_2 at temperatures below the initiation of 'silicate melting' should be noted, whereas both the oxides diminish steadily with enhanced carbonated silicate melting. After the appearance of silicate-rich melts, the Mg-numbers of garnets increase with rising temperature, as indicated by increasing MgO and decreasing FeO*. The symbols and error bars are same as in Fig. 3.

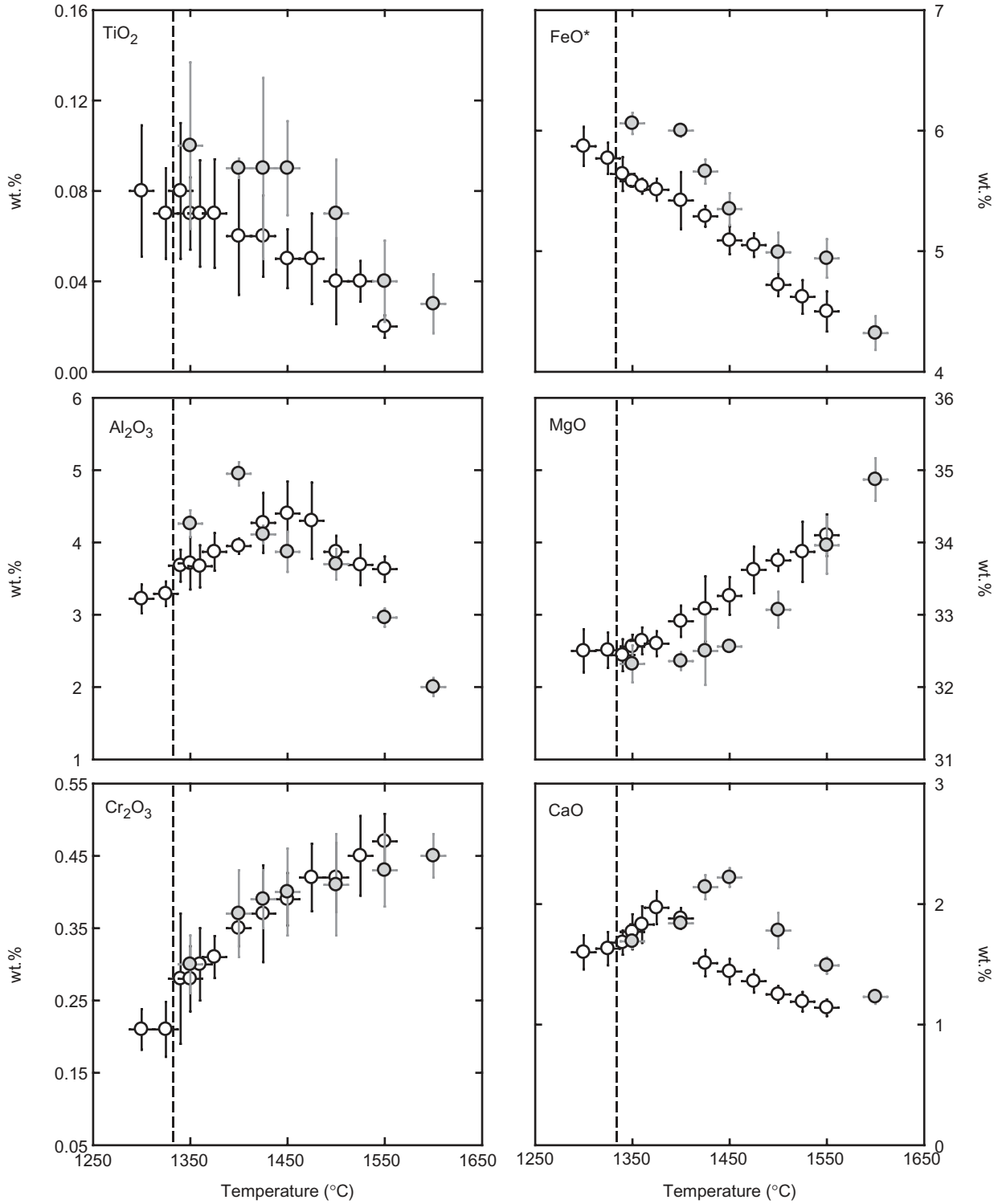

Fig. 5. Compositions of orthopyroxene from PERC and PERC3 carbonated peridotite partial melting experiments. The dashed vertical line marks the temperature of initiation of 'silicate melting' based on experiments with PERC. The symbols and error bars are same as in Fig. 3.

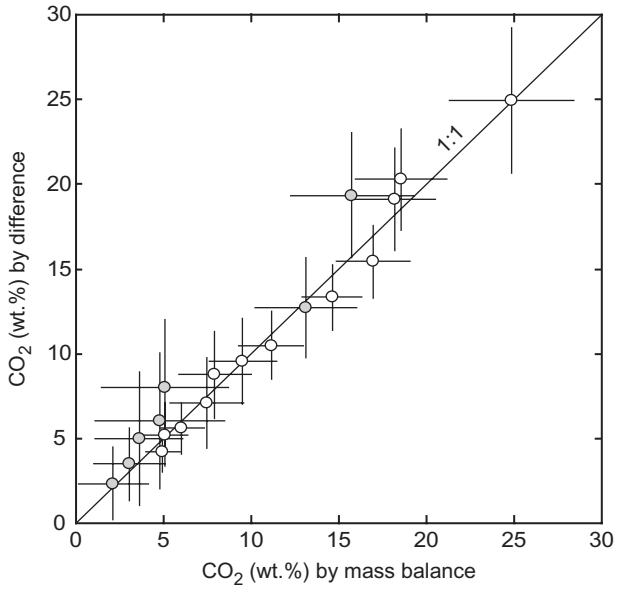

Fig. 6. Estimates of CO_2 concentration in the partial melts derived from PERC (white cricles) and PERC3 (grey circles) carbonated peridotite based on differences between 100% and average analytical totals from replicate electron microprobe analyses vs the CO_2 concentrations estimated from melt proportion derived from mass-balance calculation and the assumption that all the carbon in the charge resides in the partial melt when crystalline carbonate is absent. The error bars in CO_2 derived from microprobe totals reflect the 1σ (wt%) uncertainties in the analytical totals, and the error bars in CO_2 estimates from mass-balance calculations are based on uncertainties in estimated phase proportions (Table 2). Close adherence of the data to the 1:1 line indicates good agreement between the two methods and lends confidence to our estimates of CO_2 concentrations in quenched carbonated silicate melts.

21·7 wt% with fairly constant Mg-number of 85–86. CaO concentrations in PERC garnet increase from ~4·5 at 1105°C to 5·6 at 1340°C in the presence of calcio-dolomitic carbonatite, but then decrease steadily to ~4·7 wt% at 1425°C with increasing degree of carbonated silicate melting.

Orthopyroxene

Compositions of aluminous orthopyroxene vary systematically across the melting interval of PERC and PERC3 at 3 GPa (Table 6, Fig. 5). From 1340°C to 1450°C the Al_2O_3 content of opx increases with temperature from 3·3 to 4·4 wt% and then, after the disappearance of garnet (1425–1450°C), it decreases to 3·6 at 1550°C. PERC3 opx shows a similar trend, with Al_2O_3 increasing in the presence of garnet, from ~4·3 wt% at 1350°C to ~5 wt% at 1400°C and then diminishing to 2·0 wt% at 1600°C. CaO in PERC opx also increases from ~1·6 wt% at 1325°C to ~2·0 wt% at 1375°C and then decreases to 1·1 wt% at 1550°C. For PERC3, CaO content in opx also increases with temperature while cpx and garnet are present, but then decreases with temperature with increasing melt fraction. A steady decrease of TiO_2, Cr_2O_3 and FeO*, and increase of MgO, is also observed with increasing temperature and melt fraction.

Olivine

For PERC, the Mg-number of olivine increases steadily with increasing temperature from ~89·8 near the solidus at 1075–1105°C to ~93·4 at 1600°C (Table 7). For PERC3, the Mg-number in olivine increases across the carbonated silicate meting interval from 89·8 at 1350°C to 93·6 at 1600°C.

DISCUSSION

Comparison with previous partial melting experiments on carbonated peridotite

Experimental determinations of compositions of silicate partial melt derived from carbonated peridotite are limited. The only analyses of silicate partial melt of natural peridotite in the presence of CO_2 and in the carbonate stability field are from Hirose (1997), who investigated phase relations of KLB-1 peridotite + 5% magnesite (2·6 wt% bulk CO_2: Table 1) at 3 GPa. The partial melts are similar to those derived from PERC, with the chief difference that the partial melts of KLB-1 + magnesite are more magnesian than the partial melts of PERC3 and PERC at any given extent of melting. Also, the partial melts from PERC are richer in FeO* at a given MgO content than those from carbonated peridotite of Hirose (1997).

Compositions of partial melt from natural carbonated peridotite can also be compared with composition of liquids produced in model peridotite CMAS + CO_2 multiple saturation experiments (Dalton & Presnall, 1998*a*; Gudfinnsson & Presnall, 2005), although the pressures of these studies (3·2–8 GPa) are greater than that in the present study. In general, liquids from the natural and CMAS + CO_2 studies have a number of common features, including decreasing molar Ca/(Ca + Mg), CaO and CO_2, and increasing SiO_2 with increasing temperature. For example, between 1350 and 1600°C at 3 GPa, Ca/(Ca + Mg) decreases from 0·48 to 0·15 for PERC and from 0·44 to 0·17 for PERC3; between 1405 and 1505°C at 6 GPa, Ca/(Ca + Mg) decreases from 0·37 to 0·29 (Dalton & Presnall, 1998*a*). However, in detail the natural and CMAS + CO_2 silicate partial melts are distinct. The most apt direct comparison for the 3 GPa data is with the 3·2–3·3 GPa experiments of Gudfinnsson & Presnall (2005), and at a similar temperature these have higher molar Ca/(Ca + Mg) and significantly lower SiO_2 and Al_2O_3 than partial melts from natural bulk compositions (this study; Hirose, 1997). The lower molar Ca/(Ca + Mg) of silicate partial melts derived from natural carbonated peridotite with respect to those derived from CMAS + CO_2 bulk composition, at a given pressure and temperature, is possibly due to the lower CO_2

Table 8: Melting reactions (in weight units) for generation of silicate melts from peridotite ± CO_2 at 3 GPa

Reference	Bulk composition	Melting interval	Melting reactions	Reaction number
This study	PERC	cbL-out to cpx-out: 10–13%	1·0 ol + 1·4 cpx = 1·1 opx + 0·3 gt + 1·0 sL	(1)
		cpx-out to gt-out: 13–23%	1·0 gt = 1·0 sL	(2)
		gt-out to opx-out: 23–50%	1·1 opx = 0·1 ol + 1·0 sL	(3)
	PERC3	cbL-out to cpx and gt-out: 6–19%	1·0 cpx + 0·6 gt + 0·3 ol = 0·9 opx + 1·0 sL	(4)
		cpx and gt-out to opx-out: 19–47%	0·2 ol + 0·8 opx = 1·0 sL	(5)
Hirose (1997)	KLB-1 + 5% mst	cpx-out to gt-out: 18–28%	0·1 ol + 0·3 opx + 0·6 gt = 1·0 sL	(6)
Walter (1998)	KR4003	solidus to gt-out: 0–10%	0·1 ol + 0·8 cpx + 0·3 gt = 0·2 opx + 1·0 sL	(7)
		gt-out to cpx-out: 10–23%	0·1 ol + 1·5 cpx = 0·6 opx + 1·0 sL	(8)
		cpx-out to opx-out: 23–50%	0·0 ol + 1·0 opx = 1·0 sL	(9)

cbL, carbonate-rich melt; sL, carbonated silicate melt.

content of the former, as CO_2 influences the CaO content of carbonated silicate partial melts, as discussed in detail below.

Melting phase relation of carbonated peridotite at 3 GPa

Melting reactions

Based on the calculated phase proportions in each run (Table 2; Fig. 2) and following the method of Walter *et al.* (1995), we obtained the average melting reactions for carbonated peridotites PERC and PERC3 at 3 GPa in terms of mass units (Table 8). For both PERC and PERC3, carbonated silicate melt is initially produced by reaction of carbonatitic melt, cpx, and garnet and precipitation of opx. For PERC, the first silicate mineral to be exhausted is cpx at 1350–1360°C, and this results in further precipitation of opx and enhanced production of carbonated silicate melt [Table 8: reaction (1)]. For both the bulk compositions, garnet is the primary contributor to silicate melt generation, following the exhaustion of cpx [Table 8: reactions (2) and (4)], leading to alumina enrichment in the carbonated silicate partial melts. With further increases in temperature, the CO_2 contents of partial melts diminish and melt fraction increases with opx entering the melt phase.

The order of exhaustion of silicate phases in the PERC melting experiments is similar to that found by Hirose (1997) for KLB1 +5% magnesite; for both the bulk compositions garnet is the predominant contributor to melt production from ~15 to 30% melting. Comparison of 3 GPa melting reactions of peridotite in the presence (2·6% CO_2: Hirose, 1997; 2·5% CO_2: PERC, this study; 1·0% CO_2: PERC3, this study) and in the absence of CO_2 (Walter, 1998) indicates that increasing CO_2 suppresses the stability field of cpx relative to silicate partial melts (Table 8). Also, with decreasing bulk CO_2 garnet enters the silicate melt phase in preference to cpx, enhancing the Al_2O_3 content of small-degree silicate partial melts of CO_2-poor peridotite.

Effect of carbonate on partial melting of peridotite

As has been shown previously (Wyllie & Huang, 1976; Eggler, 1978; Falloon & Green, 1989; Dasgupta & Hirschmann, 2006), a principal effect of carbonate on the partial melting of peridotite is the drastic lowering of the solidus. The solidus temperatures (1075–1105 °C for PERC and ~1050°C for PERC3) at 3 GPa are similar to those previously observed for natural carbonated peridotite (Falloon & Green, 1989) and consistent with similar solidus lowering observed for the PERC and PERC3 bulk compositions at 6·6 GPa (Dasgupta & Hirschmann, 2007). The large decrease in solidus temperature is caused primarily by stabilization of carbonatitic melt at the solidus of peridotite, but the onset of silicate melting also occurs well below the solidus of volatile-free peridotite. Carbonated silicate partial melts are produced from PERC and PERC3 at ~1350°C, 120–150°C lower than the 3 GPa solidus of peridotite in the absence of CO_2 (Herzberg *et al.*, 2000; Hirschmann, 2000). Carbonated silicate partial melts of KLB-1 peridotite + 5% magnesite at 3 GPa appear at slightly higher temperature, between 1350 and 1400°C (Hirose, 1997). This slightly more refractory behavior found by Hirose is probably due to the addition of carbonate as magnesite rather than the Mg + Ca + Fe + Na carbonate mixture used to construct PERC and PERC3. For CMAS + CO_2 systems,

the transition from carbonatite to carbonated silicate melts occurs at a distinctly higher temperature (1500 ± 50°C at 3·2 GPa: Gudfinnsson & Presnall, 2005) than those observed for natural compositions (this study; Hirose, 1997). The lower temperature of carbonated silicate melting for the more complex bulk compositions must be due to the effects of alkalis, TiO_2 and FeO*, which stabilize carbonated silicate melts at lower temperatures. The difference in temperature of carbonated silicate melting between CMAS + CO_2 and natural peridotite + CO_2 systems near 3 GPa (*c.* 150 ± 50°C) is comparable with the temperature difference between the volatile-free solidus in the two systems [at 3 GPa CMAS: 1570°C (Presnall *et al.*, 2002), peridotite: ~1475°C (Hirschmann, 2000)].

From the onset of melting, the melt fraction of carbonatite produced is limited by the total availability of carbonate. Thus, following elimination of solid carbonate (magnesite or dolomite) from the residue, increases in melt fraction with temperature are proportional to the increase in dissolved silicate fraction. Consequently, the transition from true carbonatite to carbonated silicate melts corresponds to a large increase in the isobaric melt productivity for both PERC and PERC3 (Dasgupta *et al.*, 2007).

Effect of CO_2 on compositions of partial melts of peridotite

Differences between the compositions of carbonated silicate partial melts of volatile-poor peridotite and carbonated peridotite have been explored previously based on simple system experiments (Eggler, 1978; Dalton & Presnall, 1998*a*; Gudfinnsson & Presnall, 2005) and a limited number of experiments on natural carbonated peridotite (Hirose, 1997). The most striking differences between the compositions of partial melts of carbonated peridotite at 3 GPa and those of CO_2-free peridotite at similar pressures (Hirose & Kushiro, 1993; Walter, 1998) are increased CaO and diminished SiO_2, both of which we will consider in some detail. Additionally, CO_2 may influence the Fe–Mg partitioning between melts and residual minerals, thereby influencing the FeO* of partial melts.

Effect of CO_2 on SiO_2 in partial melts

It has long been known that addition of CO_2 diminishes the SiO_2 content of partial melts of peridotite (Eggler, 1978). In Fig. 7a we plot wt% SiO_2 vs wt% CO_2 for the partial melts in our experiments, together with carbonated silicate and carbonatite liquids produced in other partial melting experiments on natural and model peridotite systems. The data from other studies are chiefly at 3 GPa, but also include higher pressure data up to 8 GPa (see figure caption for details). All liquids are in equilibrium with olivine and orthopyroxene. The data define a single trend of decreasing SiO_2 concentrations with increasing CO_2 with a slope very close to −1. However, liquids from PERC3 plot above the trend, reflecting more SiO_2 in these partial melts than expected for the observed concentrations of CO_2. This is particularly evident when the compositions are cast as oxide mole fractions (Fig. 7b), as the PERC3 trend then appears to have a different slope compared with data from PERC and from other studies. On the other hand, when the data are cast as wt% oxides (Fig. 7a), it is only the two lowest melt fractions that appear as convincing outliers. The reason for the different trend for the PERC3 experiments is unclear, but it may be due to the difficulty of obtaining accurate melt compositions for the small melt fractions (6 and 8%; Table 2) in these experiments. Interestingly, carbonated silicate and carbonatite melts plot on the same trend, suggesting that the mixing mechanism between CO_2 and silicate melt is similar for carbonatites and for high-pressure alkalic silicate liquids.

The inverse relationship between SiO_2 and CO_2 in partial melts of carbonated peridotite does not depend strongly on temperature, pressure, or other compositional parameters such as the concentration of Al_2O_3 or alkalis. This is not surprising. Although pressure is known to have a significant effect on the SiO_2 content of partial melts of peridotite at low pressure (Albarède, 1992; Langmuir *et al.*, 1992; Hirose & Kushiro, 1993), this dependence is small at pressures above 3 GPa (Walter, 1998). Similarly, large changes in temperature and extent of melting have a modest effect on the SiO_2 concentration in partial melts of volatile-poor garnet peridotite from 3 to 7 GPa (Walter, 1998). Finally, concentrations of alkalis in the liquid have a modest effect at 3 GPa (Hirschmann *et al.*, 1998) and the relatively small variations in TiO_2 among partial melts in Fig. 3 (0–2 wt%) may account for only modest (~1 wt%) changes in SiO_2 concentrations (Xirouchakis *et al.*, 2001).

The inverse relationship between mole fractions of SiO_2 and CO_2 observed for peridotite partial melts is in part the result of dilution. Increases in dissolved CO_3^{2-} ions, accompanied by associated cations (chiefly Ca^{2+}, Mg^{2+}, Fe^{2+}, Brooker *et al.*, 2001) must dilute the proportion of SiO_2 in the melt and so it may be expected that a plot of X_{SiO_2} vs X_{CO_2} should yield a slope close to −1. However, it should be remembered that all of the liquids plotted in Fig. 7 are in equilibrium with olivine and orthopyroxene. Thus the activity of silica, a_{SiO_2}, is buffered by the coexistence of olivine and orthopyroxene

$$\underset{\text{opx}}{Mg_2Si_2O_6} \leftrightarrow \underset{\text{melt}}{SiO_2} + \underset{\text{olivine}}{Mg_2SiO_4} \qquad (1)$$

and therefore liquids with very different values of X_{SiO_2} have similar values of a_{SiO_2}. The maintenance of near-constant a_{SiO_2} in the face of substantial dilution by carbonate is not the expected behaviour for a thermodynamically ideal solute. Rather it requires strong excess free

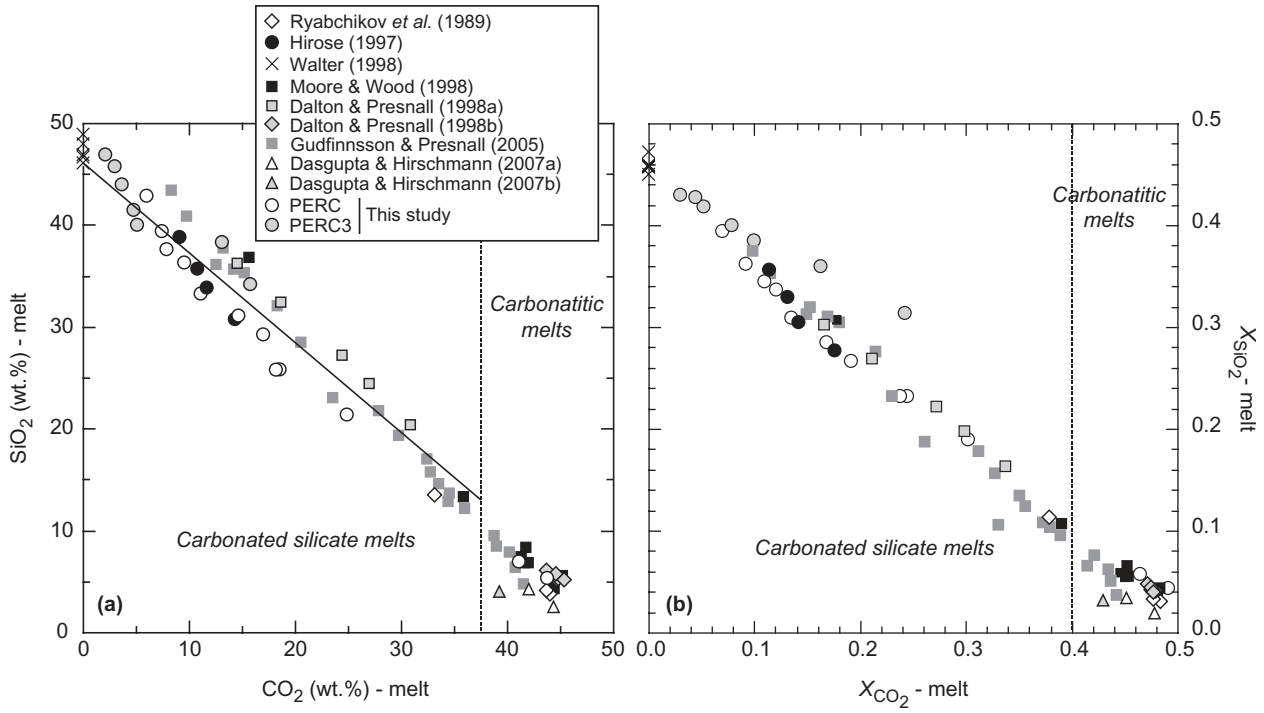

Fig. 7. Measured concentrations of SiO_2 vs estimated concentrations of CO_2 in carbonatite and carbonated silicate partial melts from this study and other studies in simple (Dalton & Presnall, 1998*a*, 1998*b*; Moore & Wood, 1998; Gudfinnsson & Presnall, 2005) and complex (Ryabchikov *et al.*, 1989; Hirose, 1997; Walter, 1998; Dasgupta & Hirschmann, 2007*a*, 2007*b*) peridotite ± CO_2 compositions from 2·8 to 8 GPa in terms of weight per cent (a) and oxide mole fraction (b). For the experiments of Hirose (1997), melt CO_2 concentrations are estimated as described in the caption to Fig. 3. All melts coexist with olivine and orthopyroxene, and consequently all have silica activity buffered. The linear fit of the melt compositions between 0 and 37 wt% CO_2 in the melt is given by $C^{liq}_{SiO_2} = 46 \cdot 2 - 0 \cdot 89 C^{liq}_{CO_2}$, where $C^{liq}_{SiO_2}$ and $C^{liq}_{CO_2}$ are weight concentrations of SiO_2 and CO_2 in the melt. It should be noted that these SiO_2 concentrations are not normalized on a volatile-free basis, whereas melt SiO_2 concentrations in Figs 3, 9, 12 and 14 and in Table 3 are normalized to volatile-free compositions. This linear parameterization allows estimation of the SiO_2 concentrations of model melts as a function of bulk CO_2 content and extent of melting that is presented in Fig. 14.

energies of mixing between SiO_2 and dissolved CO_2. On the other hand, near-constant activity of a component at highly variable concentration is generally expected in solutions that are close to immiscibility. Of course, high-temperature immiscibility between silicate and carbonate liquids is well documented (Lee & Wyllie, 1997; Dasgupta *et al.*, 2006).

Effect of CO_2 on CaO in partial melts

Concentrations of CaO in partial melts of nominally volatile-free peridotite vary significantly, depending on whether cpx is exhausted from the residue, the melt fraction, and other factors, such as concentrations of alkalis in the melt (Hirschmann *et al.*, 1999). At 3 GPa, partial melts from experiments on volatile-free peridotite have CaO concentrations of up to 10·7 wt% (Hirose & Kushiro, 1993; Walter, 1998; Kushiro, 2001). In contrast, partial melts of carbonated peridotite have CaO concentrations that increase with increasing CO_2 in the melt and reach 25 wt% (Fig. 8a). At low concentrations of CO_2 (below 10 wt%), the trends for PERC and PERC3 are distinct, with the latter showing greater increases in CaO for a given concentration of CO_2 in the melt. Carbonated silicate and carbonatite liquids produced in other partial melting experiments with natural and model peridotite systems at 3–8 GPa also show increased CaO with increasing dissolved CO_2 (Fig. 8).

Some of the liquids from the present experiments and from previous studies are in equilibrium with clinopyroxene, orthopyroxene and olivine, meaning that the activity of CaO in these liquids, a_{CaO}, is buffered by reaction between the melt and coexisting minerals:

$$2\underset{\text{melt}}{CaO} + 3\underset{\text{opx}}{Mg_2Si_2O_6} \leftrightarrow \underset{\text{cpx}}{2CaMgSi_2O_6} + \underset{\text{olivine}}{2Mg_2SiO_4}. \quad (2)$$

This buffering reaction limits a_{CaO} to similar values for lherzolite-saturated liquids, but with increasing dissolved CO_2, such liquids have greater concentrations of CaO (Fig. 8b). Consequently, the increases in CaO concentration that accompany increased CO_2 must be owing to decreases in the activity coefficient of CaO as it reacts with dissolved CO_2 to form $CaCO_3$ complexes according to

$$\underset{\text{melt}}{CaO} + CO_2 \leftrightarrow \underset{\text{melt}}{CaCO_3}. \quad (3)$$

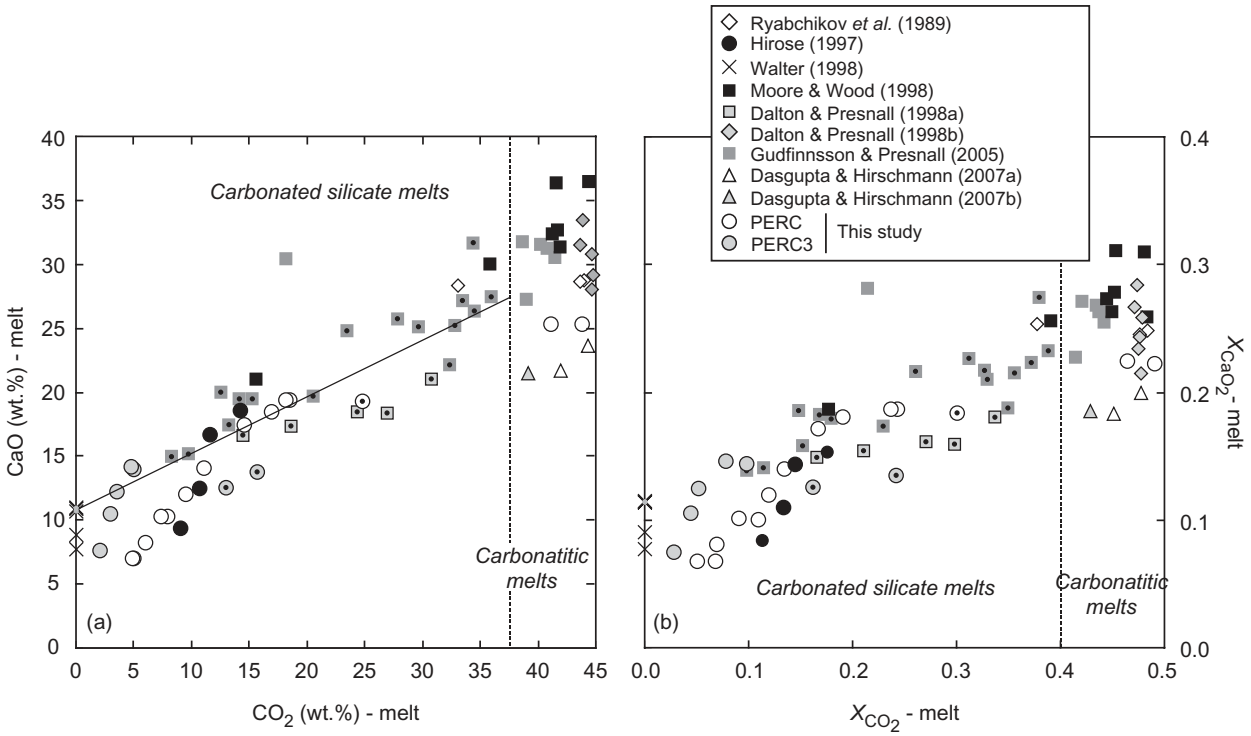

Fig. 8. Measured concentration of CaO vs estimated concentration of CO_2 in carbonatite and carbonated silicate partial melts from this study and other studies in simple and complex peridotite ± CO_2 compositions in terms of weight per cent (a) and oxide mole fraction (b). The linear fit of the lherzolite saturated melt compositions (cpx-present runs are indicated by circular symbols with central dots) between 0 and 37 wt% CO_2 in the melt is given by 'melt $C^{liq}_{CaO} = 10 \cdot 7 + 0 \cdot 44 C^{liq}_{CO_2}$, where C^{liq}_{CaO} and $C^{liq}_{CO_2}$ are the CaO and CO_2 concentrations in the melt. It should be noted that these CaO concentrations are not normalized on a volatile-free basis, whereas CaO concentrations in Figs 3, 9, 12 and 14 and in Table 3 are normalized to volatile-free compositions. This linear parameterization allows estimation of the CaO concentrations of model melts as a function of bulk CO_2 content and extent of melting that is presented in Fig. 14. The data sources are same as in Fig. 7.

This speciation of Ca, which is in agreement with spectroscopic data that suggest that CO_3^{2-} ligands in silicate liquids complex preferentially with Ca^{2+} cations (Brooker *et al.*, 2001), reduces the activity coefficient of CaO and consequently increases the stability of Ca in the melt.

Many partial melting experiments on natural carbonated peridotite from this study and all of those from Hirose (1997) produced relatively high melt fractions in which melt coexisted with a garnet harzburgite, rather than a garnet lherzolite residue. In these experiments, a_{CaO} is not buffered by reaction (2), but reductions in a_{CaO} by dissolved CO_2 allow large concentrations of CaO without forcing saturation in cpx. Thus, increased amounts of dissolved CO_2 in carbonated partial melts in equilibrium with harzburgite residue also enhance CaO concentrations (Fig. 8). In effect, the low activity coefficients of CaO in carbonated partial melts allow Ca to behave as a highly incompatible element during partial melting of harzburgite. Thus, for partial melts in equilibrium with a harzburgitic residue, the concentration of CaO in the melt depends on the melt fraction as well as the concentration of CO_2 in the melt, and at high melt fractions, the former becomes more important than the latter. This explains why the trends for PERC and PERC3 are distinct in Fig. 8. The two bulk compositions have similar CaO concentrations, but PERC has more CO_2 (Table 1). Consequently, at a given melt fraction coexisting with a harzburgitic residue, partial melts of the two bulk compositions will have similar CaO concentrations, but those for PERC will be richer in CO_2.

CaO vs SiO_2

The concentration of dissolved CO_2 is a key factor leading to enhanced CaO and diminished SiO_2 in partial melts of peridotite. Thus, for a given bulk composition, partial melts generated at low melt fraction are most enriched in CaO and depleted in SiO_2, as these have the greatest concentrations of dissolved CO_2 (Fig. 9). However, as noted above, CaO is also influenced by melt fraction. Consequently, PERC and PERC3 follow distinct trends on a plot of CaO vs SiO_2 owing to their different bulk CO_2 concentrations (Fig. 9). The importance of these

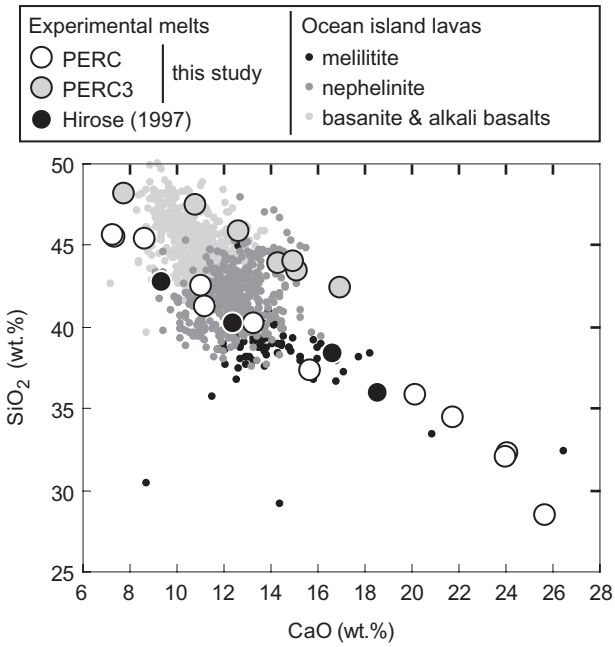

Fig. 9. Normalized CaO (wt%) vs SiO_2 (wt%) for silicate partial melts of carbonated peridotite from this study and from Hirose (1997) compared with those of melilitites, nephelinites, basanites, and alkali basalts from oceanic islands (GEOROC database: http://georoc.mpch-mainz.gwdg.de/georoc/). The CaO–SiO_2 trend for partial melts from PERC3 is distinct from those of PERC and Hirose (1997), which suggests that CaO–SiO_2 relations depend on the bulk CO_2 concentration of peridotite sources.

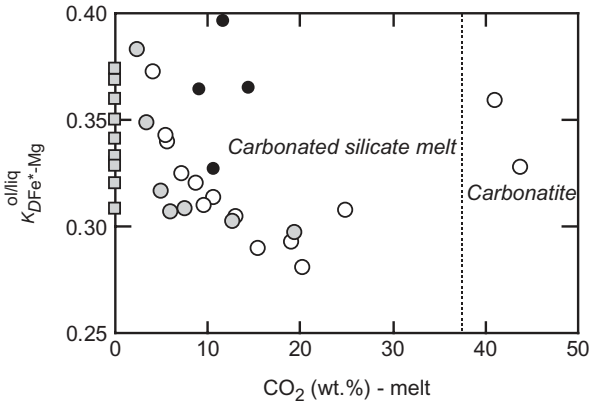

Fig. 10. Olivine–liquid Fe*–Mg distribution coefficient, $K_{DFe^*-Mg}^{ol/liq}$ as a function of CO_2 concentration (wt%) in partial melts of carbonated peridotite at 3 GPa (this study and Hirose, 1997) compared with results for nominally CO_2-free silicate melts at the same pressure (Ulmer, 1989; Hirose & Kushiro, 1993; Walter, 1998). For experiments of Hirose (1997), melt CO_2 concentrations are estimated as described in the caption to Fig. 3. A slight dependence of decreasing $K_{DFe^*-Mg}^{ol/liq}$ with increasing concentration of melt CO_2 content is apparent from our data; however, the average values of $K_{DFe^*-Mg}^{ol/liq}$ remains similar to that for olivine-basaltic melt equilibria.

distinct trends to the petrogenesis of alkalic OIB is considered below.

Effect of CO_2 on Fe–Mg partitioning between olivine and silicate melt*

The equilibrium constant for Fe*–Mg partitioning between olivine and silicate melts, $K_{DFe^*-Mg}^{ol/liq}$, is normally close to 0·3 at low pressure (Roeder & Emslie, 1970) and increases gently with pressure (Ulmer, 1989; Toplis, 2005); however, variations in melt composition can yield both higher and lower values (Longhi *et al.*, 1978; Gee & Sack, 1988; Baker *et al.*, 1995; Toplis, 2005). For carbonated silicate liquids from this study ranging from 2 to 25 wt% CO_2, the average value is $0{\cdot}32 \pm 0{\cdot}03$, close to the canonical value. In detail, however, there is a weak trend of decreasing $K_{DFe^*-Mg}^{ol/liq}$ with increasing X_{CO_2}, although the scatter of the data is too great to yield a statistically valid correlation (Fig. 10). Thus, the influence of CO_2 on $K_{DFe^*-Mg}^{ol/liq}$ is small, despite large apparent variations in melt structure. It is not clear whether this effect can be analyzed in terms of models that posit a strong influence of melt silica concentration (Toplis, 2005) or melt polymerization (Kushiro & Mysen, 2002) on $K_{DFe^*-Mg}^{ol/liq}$. Whereas an increase in dissolved CO_3^{2-} reduces SiO_2 in the melt and polymerizes the aluminosilicate portion of the melt by converting non-bridging oxygens to bridging oxygens, it also provides new bonding environments in which Fe^{2+} and Mg^{2+} can associate with CO_3^{2-}.

Interestingly, the trend to lower $K_{DFe^*-Mg}^{ol/liq}$ with increasing CO_2 for carbonated silicate melts is distinct from the large values of $K_{DFe^*-Mg}^{ol/liq}$ observed when carbonatite liquid coexists with olivine (Dalton & Wood, 1993; this study). This difference is not surprising given strong Fe^{2+}–Mg partitioning between coexisting carbonatite and carbonated silicate liquids (Dasgupta *et al.*, 2006).

Origin of highly alkalic basalts

Possible role of carbonated peridotite in origin of natural alkalic basalts

We now consider whether partial melts of carbonated peridotite may be suitable parents to natural alkalic OIB. To aid this discussion, it is useful to distinguish highly alkalic melilitites and nephelinites from moderately alkalic basalts and basanites, based on the chemical classification of LeBas (1989). The distinctions between these groups are largely arbitrary, as lavas grade continuously from one to the other. However, melilitites are strikingly rich in CaO and low in SiO_2 (Fig. 9), and therefore have the characteristics most likely to be associated with a strong role for carbonated silicate partial melts of peridotite. Alkali basalts and basanites have much lower CaO and higher SiO_2, and nephelinites are intermediate between melilitites and basanites (Figs 9 and 11).

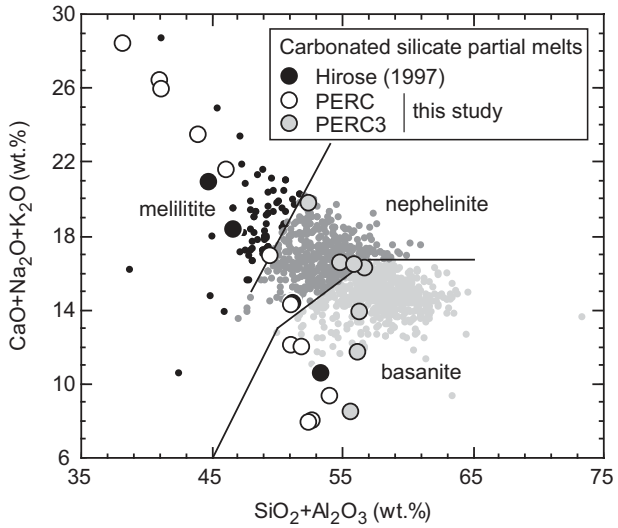

Fig. 11. Classification of alkalic to strongly alkalic ocean island lavas (GEOROC database: http://georoc.mpch-mainz.gwdg.de/georoc/) as melilitites, nephelinites, and basanites, following the scheme of LeBas (1989). Also plotted are carbonated silicate partial melts of peridotite derived from this study and from Hirose (1997).

Figure 12 shows the compositions of basanites, nephelinites, and melilitites from oceanic islands, with data from the compilation of Dasgupta *et al.* (2006). Ideally, one should compare experimental partial melts with the primary liquids that are parental to alkalic OIB, but, unfortunately, little work has been done to define the major element characteristics of such liquids. For the Cape Verde Islands, Holm *et al.* (2006) examined major element trends that suggest nephelinitic and basanitic parental magmas with >11·5 wt% MgO, 38–45 wt% SiO_2, 10–12 wt% Al_2O_3, 10·5–14·5 wt% CaO, 11–13·5 wt% FeO*, and 3–6 wt% TiO_2. In general, suites of alkalic lavas from OIB localities extend to MgO of 12 wt% or higher (Fig. 12), indicating that the primary magmas are highly magnesian. However, because such lavas are commonly laden with phenocrysts, it is difficult to distinguish very primitive liquids from lavas that have undergone crystal accumulation.

We have not attempted to define parental liquids from the trends among natural lavas in Fig. 12, but rather seek to compare experimental partial melts with primitive lavas that may plausibly be near-primary. For purposes of comparison with natural lavas, the experimental partial melts are recalculated to 100 wt% on a CO_2-free basis. We note that, except for Al_2O_3, most oxides do not show strong variation with MgO in lavas with > 8% MgO; this means that fractionation has only small effects on most oxides when only samples with > 8 wt% MgO are considered. This is presumably because the variations in oxide concentrations between different parent magmas are greater than the influence of olivine ± cpx fractionation on their differentiates. Systematic increases in Al_2O_3 with diminishing MgO indicate that parental liquids have < 12 ± 2 wt% Al_2O_3 for MgO content of ~12 wt%.

The major element compositions of experimental partial melts generated in this study are MgO-rich and in this regard are plausible candidates to be parental to alkalic OIB (Fig. 12). Partial melts of PERC have more than 19 wt% MgO and hence would require fractionation of olivine ± clinopyroxene to produce alkalic OIB, which typically have < 15 wt% MgO. Some extreme OIB have up to ~ 20 wt% MgO, but as already noted, these may not represent true liquids. Partial melts of PERC3 at < 20% melting are a little less magnesian (15–16 wt% MgO), and so may require less fractionation to approach the MgO concentrations of primitive alkalic OIB.

At 10–22% melting, partial melts of PERC are melilititic, although their compositions are more extreme than those of natural melilitites, particularly at lower melt fractions (Fig. 11). At higher extents of partial melting (> 22%), the partial melts become nephelinitic, and then above ~ 30% partial melting they are basanitic or alkali basaltic. Partial melts from the study of Hirose (1997) follow a similar trend. Partial melts of PERC3 range from compositions similar to nephelinites at low melt fractions (5–16%) to basanites at higher melt fractions (Fig. 11).

In Fig. 12, the compositions of alkalic OIB are compared with partial melts of carbonated garnet lherzolite at 3 GPa from this study and from Hirose (1997) as well as with partial melts of nominally CO_2-free garnet lherzolite at 2·5–5·0 GPa (Takahashi, 1986; Hirose & Kushiro, 1993; Kushiro, 1996; Walter, 1998). In contrast to the partial melts of volatile-free peridotite, which are richer in SiO_2 than most basanites and much richer in SiO_2 than nephelinites and melilitites, the partial melts of carbonated peridotite span the range of SiO_2 concentrations found in these highly undersaturated magmas. Also, whereas the partial melts of volatile-free lherzolite are too low in CaO and CaO/Al_2O_3 to account for the compositions of nephelinites and melilitites from oceanic islands (but possibly can account for CaO and CaO/Al_2O_3 of the basanites), the partial melts of carbonated peridotite are notably enriched in CaO and CaO/Al_2O_3. Thus, the partial melts of carbonated lherzolite have some of the key compositional features of lavas that are not easily explained by partial melting of garnet lherzolite in the absence of CO_2. Additionally, the partial melts of carbonated peridotite extend to FeO*-rich and Al_2O_3-poor compositions that may be appropriate for liquids parental to alkalic OIB, although the partial melts are not as FeO* rich as some of the most extreme lavas. Such features are also found in some of the partial melts of nominally volatile-free peridotite from the study of Walter (1998), although these derive from 5 GPa rather than the 3 GPa pressure of

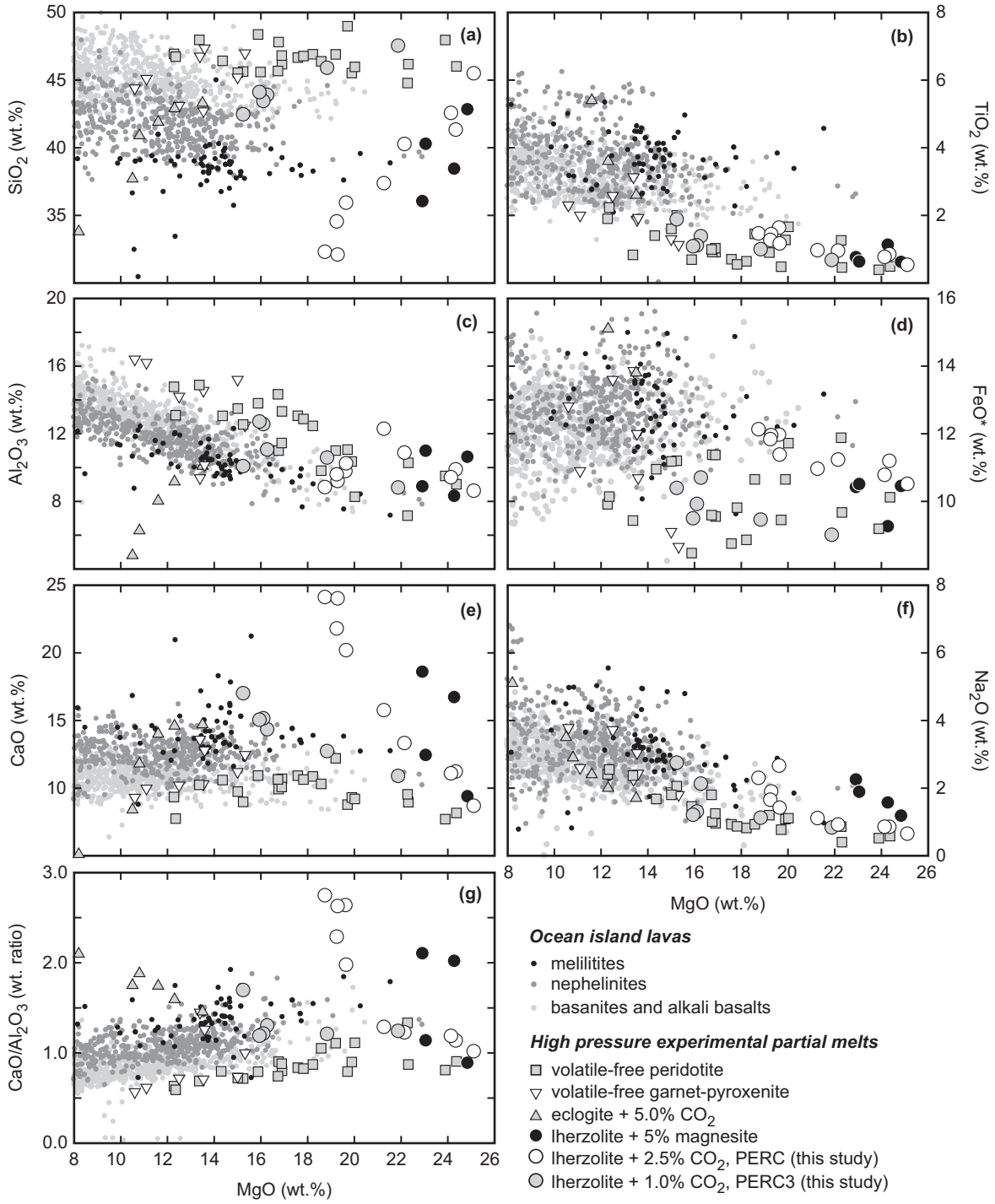

Fig. 12. Compositions of alkalic ocean island basalts compared with experimental partial melts of carbonated peridotite at 3 GPa (PERC and PERC3: this study; KLB-1 +5% magnesite: Hirose, 1997). Also shown are high-pressure experimental partial melts from volatile-free peridotite KLB-1 (Takahashi, 1986; Hirose & Kushiro, 1993), PHN1611 (Kushiro, 1996), KR4003 (Walter, 1998) between 2·5 and 5 GPa, volatile-free garnet pyroxenite MIX1G between 2 and 5 GPa (Hirschmann *et al.*, 2003; Kogiso *et al.*, 2003), and carbonated eclogite SLEC1 at 3 GPa (Dasgupta *et al.*, 2006). Data sources for natural lavas are from the compilation of Dasgupta *et al.* (2006) with additional data from Holm *et al.* (2006).

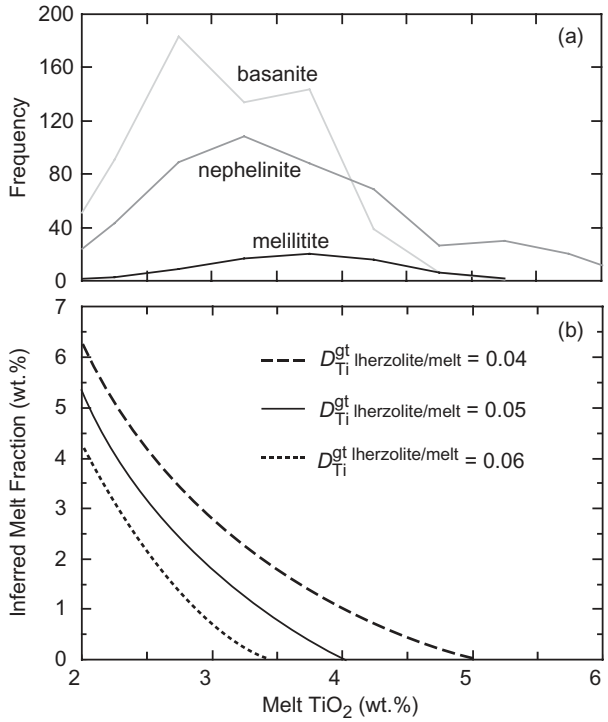

Fig. 13. (a) Frequency distribution for TiO_2 concentrations of basanitic, nephelinitic, and melilititic OIB depicted in Fig. 12, and (b) relations between concentration of TiO_2 and the extent of melting of fertile peridotite used to estimate melt fractions in sources of highly alkalic lavas in Fig. 14. Melt fractions in (b) are based on batch melting of garnet lherzolite with bulk TiO_2 content equal to 0·2 wt%, which is that of the primitive mantle (McDonough & Sun, 1995) and $D_{Ti}^{gt\ lherzolite/melt}$ ranging from 0·04 to 0·06, estimated based on experiments from this study and that of Walter (1998). The overall high concentrations of TiO_2 in these lavas (a) require small-degree partial melting if we assume a normal peridotite source and that nephelinites and melilitites are, on average, enriched in TiO_2 relative to basanites and hence represent smaller degree partial melts.

the carbonated peridotite experiments. Partial melting of volatile-free peridotite at 5 GPa requires high potential temperatures (>1550°C), which may not be appropriate for the geodynamic setting of highly alkalic OIB, which tend to derive from relatively low buoyancy flux plumes or from the cooler margins of more vigorous plumes (e.g. Lassiter *et al.*, 1996; Ren *et al.*, 2006).

Low melt fractions—the significance of TiO_2

A key consideration is that partial melts of garnet lherzolite and carbonated lherzolite are much lower in TiO_2 than is natural alkalic OIB. Whereas the experimental partial melts have < 2 wt% TiO_2, the basanites, nephelinites, and melilitites with > 8 wt% MgO compiled in Fig. 12 have 2–6 wt% TiO_2 and average 3·1 ± 0·6, 3·6 ± 0·6, and 3·9 ± 0·6 wt% TiO_2, respectively (n = 613, 483, and 75, respectively) (Fig. 13). These concentrations may have been enhanced a small amount by crystal fractionation, but the effect is probably minimal, as mean TiO_2 concentrations remain similarly high for even the most MgO-rich lavas (Fig. 12). This difference emphasizes that the lavas are the products of small degrees of partial melting, as noted in the Introduction, whereas the experimental partial melts are high-degree partial melts (all are products of >5% melting and most >10% melting). This difference in degree of melting may be of critical importance when comparing the melt compositions from experiments with those of natural lavas, as small-degree partial melts of carbonated lherzolite may have compositions markedly different from their higher degree counterparts because of the great increase in CO_2 concentration in the liquid expected near the solidus.

The high TiO_2 concentrations in alkalic OIB can be used to estimate the melt fractions of carbonated garnet lherzolite or garnet lherzolite that may plausibly account for liquids parental to basanites, nephelinites, and melilitites. The bulk garnet lherzolite/melt partition coefficient for Ti, $D_{Ti}^{gt\ lherzolite/melt}$, is in the range 0·04–0·06 both for carbonated lherzolite at 3 GPa (estimated for $D_{Ti}^{mineral/melt}$ values determined from this study and a garnet lherzolite with 55% olivine, 20% opx, 10% cpx, 15% garnet) and for volatile-free garnet lherzolite at 3–5 GPa [from $D_{Ti}^{mineral/melt}$ values and mineral mode data of Walter (1998)]. As shown in Fig. 13, for a garnet lherzolite source with 0·2 wt% TiO_2 similar to the primitive mantle (McDonough & Sun, 1995), liquids with 2–5 wt% TiO_2 are generated at melt fractions from ~6 to 0%. Using $D_{Ti}^{gt\ lherzolite/melt}$ of 0·04, bulk TiO_2 content of 0·2 wt%, and the TiO_2 contents of OIB plotted in Fig. 12, we have calculated the extent of melting for each OIB composition. This yields average extents of melting of 2·8 ± 1·5, 2·0 ± 1·5, and 1·7 ± 1·5%, respectively, for ocean island basanites, nephelinites, and melilitites. If $D_{Ti}^{gt\ lherzolite/melt}$ = 0·06, then the average degree of melting is below 1% for all three lava types. It should be noted that a modest fraction of nephelinites have >5 wt% TiO_2, and these can be derived from a garnet lherzolitic source only if that source is enriched in TiO_2 relative to Bulk Silicate Earth. It should be noted also that the depleted mantle composition of Workman & Hart (2005) with 0·12 wt% TiO_2 cannot produce TiO_2-rich parental lavas above 3 wt% TiO_2 at any melt fraction.

To facilitate comparison with the experimental data, we have calculated the melt fractions required to produce alkalic basalts from oceanic islands, assuming a peridotite source with 0·2 wt% TiO_2 and $D_{Ti}^{gt\ lherzolite/melt}$ of 0·04. The compositions of these lavas are plotted versus the calculated melt fractions in Fig. 14. Lower calculated melt fractions resulting from a source with lower TiO_2 or a higher value of $D_{Ti}^{gt\ lherzolite/melt}$ would not affect appreciably the comparison with the experiments. Significantly higher calculated melt fractions could result only if the

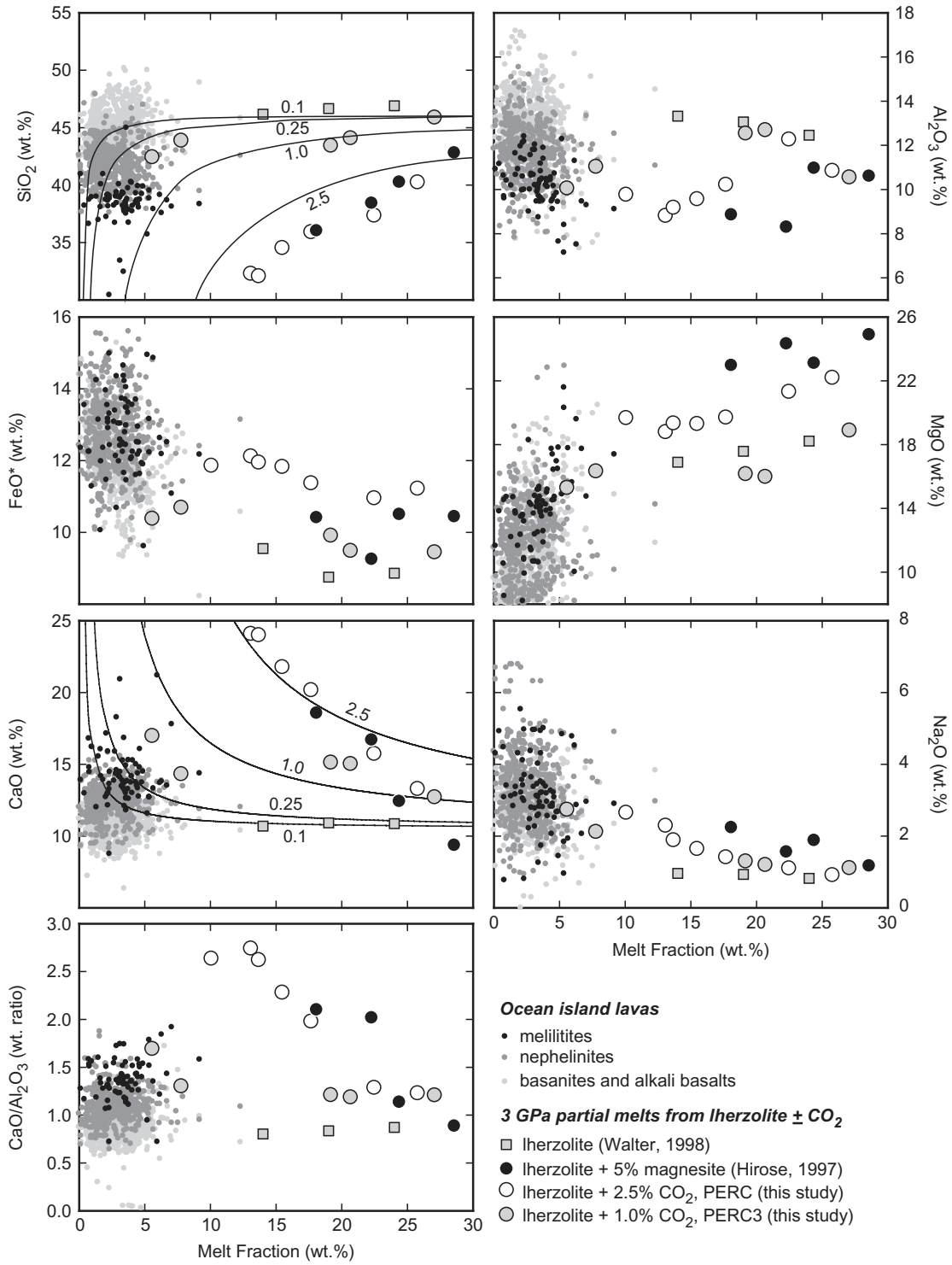

Fig. 14. Normalized major element oxide concentrations (wt%) and CaO/Al_2O_3 weight ratio for alkalic to strongly alkalic ocean island basalts plotted as a function of estimated melt fraction (wt%) and compared with 3 GPa experimental partial melts of peridotite ± CO_2 (Hirose, 1997; Walter, 1998; this study). For the experiments of Hirose (1997), melt fractions are estimated as described in the caption to Fig. 3. Extents of melting for the lavas are as described in Fig. 13, using $D_{Ti}^{gt\ lherzolite/melt}$ of 0·04. Larger partition coefficients or lower TiO_2 concentrations in the source mantle would diminish the melt fraction estimates. For the melt fraction vs SiO_2 (wt%) and CaO (wt%) diagrams, model curves for partial melting of bulk compositions with variable CO_2 content (in wt% indicated next to the curves) are included, where the relationship of melt SiO_2 (wt%) vs melt CO_2 (wt%) and melt CaO (wt%) vs melt CO_2 (wt%) are from the trends shown in Figs 7 and 8 respectively.

source were assumed to be enriched in TiO_2 compared with primitive mantle, which in turn would require a metasomatized or non-peridotitic source, such as eclogite or pyroxenite.

When partial melts of carbonated peridotite are compared with alkalic lavas based on melt fraction, several features are evident. Most notably, compared with the lavas, partial melts of carbonated peridotite with 2·5 wt% CO_2 trend to extremely low SiO_2 and high CaO and CaO/Al_2O_3. Thus, if natural OIB are derived from partial melting of carbonated peridotite, the source must have less CO_2. Compositions of partial melts of carbonated peridotite with 1 wt% CO_2 do not trend to extremely low SiO_2, high CaO and high CaO/Al_2O_3 at low melt fraction, and therefore may be more realistic candidates for the sources of alkalic OIB. However, even though they represent comparatively high melt fractions (5–8%) these partial melts of PERC3 have CaO and CaO/Al_2O_3 comparable with the most extreme melilitites. At lower melt fractions, partial melts of PERC3 probably have more extreme CaO and CaO/Al_2O_3 than the lavas. Also, as discussed above, the two lowest-degree partial melts of PERC3 (at 1400 and 1350°C) have anomalously high SiO_2 compared with melts of comparable CO_2 concentration (Fig. 7). This suggests that the compositions of the lavas may be accounted for by partial melting of peridotite with significantly less CO_2 than PERC or PERC3. On the other hand, if the SiO_2 contents of the low-degree partial melts of PERC3 are not spurious, then the experiments suggest that carbonated peridotites with sufficient CO_2 to generate the low SiO_2 contents of nephelinites and melilitites at low melt fraction will produce partial melts that are too extreme in CaO and CaO/Al_2O_3.

More experiments at low degrees of partial melting and with small amounts of added CO_2 are required to address whether small-degree partial melts of carbonated peridotite can be parental to highly alkalic OIB. For the present, we can explore some of the likely compositional features of such partial melts in a semi-quantitative fashion by using the SiO_2–CO_2 and CaO–CO_2 relationships developed in Figs 7 and 8 to model the SiO_2–F and CaO–F trends for partial melting of a peridotite with a given bulk CO_2 concentration expected at low melt fractions for peridotite with small amounts of CO_2. We note that there is considerable scatter in these trends, some resulting from experimental and analytical uncertainties, and that no simple relationship between melt CO_2, CaO, and SiO_2 could reproduce accurately both the PERC and PERC3 data.

As shown in Fig. 14, the characteristic enrichments in CaO and depletions in SiO_2 of nephelinites and melilitites may be matched by small-degree (1–5%) partial melts of peridotite with 0·1–0·25 wt% bulk CO_2. Such concentrations may be geochemically plausible (Javoy & Pineau, 1991; Dixon *et al.*, 1997; Pineau *et al.*, 2004). Partial melts that match the most extreme melilitite compositions with ~36 wt% SiO_2 and ~18% CaO would have ~12–15 wt% CO_2. There are few quantitative constraints on the likely concentrations of Al_2O_3, MgO, and FeO* expected from low-degree partial melts of carbonated peridotite. One may anticipate that Al_2O_3 concentrations diminish near the solidus, owing to the large stoichiometric proportion of garnet involved in the initial carbonated silicate melt-forming reaction (Table 8), but Al_2O_3–F trends in Fig. 14 do not allow confident extrapolation to low melt fractions. MgO concentrations generally decrease with diminishing melt fraction owing to decreasing temperature, but the relationship near the solidus of carbonated garnet lherzolite is complicated by the effects of increasing CO_2 in the liquid, which tends to enhance MgO in the liquid. Also, the relationship between temperature and melt fraction depends on the bulk CO_2 concentration (Dasgupta *et al.*, 2007). Extrapolation of the trends in Fig. 14 suggests that MgO concentrations of near-solidus liquids are in the range of 16–18 wt% MgO, but that they almost certainly depend on bulk CO_2 concentration. Concentrations of FeO* presumably are related to those of MgO, assuming that $K_{DFe^*-Mg}^{ol/liq}$ is not a strong function of melt CO_2 concentration (Fig. 10), and a crucial question is whether small-degree partial melts could be sufficiently FeO* -rich to be plausible parents to the most ferruginous primitive nephelinites and melilitites, which have 13–15 wt% FeO (Fig. 13).

Possible role of water in the generation of alkalic ocean island basalts

In addition to CO_2, oceanic island basalts have minor concentrations of H_2O and other volatiles (e.g. Dixon *et al.*, 1997) that may influence the compositions of partial melts. The well-known propensity of H_2O to lower the solidus of mantle rocks (Green, 1973; Wyllie, 1979) as well as influence the compositions of partial melts (Kushiro, 1975; Mysen & Boettcher, 1975; Wyllie, 1979; Gaetani & Grove, 1998) suggests that understanding low-degree partial melting of peridotite requires exploration of the combined effects of CO_2 and H_2O.

Estimates of water content in OIB source regions vary from ~300 to 1100 ppm (e.g. Dixon *et al.*, 1997, 2002; Bureau *et al.* 1998; Nichols *et al.*, 2002; Seaman *et al.*, 2004), which is similar to the estimates of CO_2 of 300–1300 ppm (Dixon *et al.*, 1997; Bureau *et al.*, 1998; Aubaud *et al.*, 2005, 2006), with the estimated OIB source CO_2/H_2O ratio typically varying from 2·5±1·5 (Dixon *et al.*, 1997) to ~1 (Aubaud *et al.*, 2005). Despite the presence of both CO_2 and H_2O, it is CO_2, rather than H_2O, that probably has a dominant influence on the origin of highly alkalic magmas. This is partly because H_2O is partially retained in nominally anhydrous minerals, thereby allowing CO_2 to have greater influence on the lowest degrees of partial melting (Hirth & Kohlstedt, 1996; Presnall *et al.* 2002;

Dasgupta *et al*. 2007) (provided that carbon is present as carbonate, rather than in reduced form). Thus, it is to be expected generally that CO_2/H_2O ratios should be greater than unity in primary OIB and that therefore the influence of H_2O may be subordinate to that of CO_2, although some OIB sources can be richer in H_2O than CO_2 (e.g. Pitcairn: Aubaud *et al.*, 2006).

Assuming that the partition coefficient of H_2O between peridotite residua and partial melts is $\sim 0{\cdot}009$ (Aubaud *et al.*, 2004; Hauri *et al.*, 2006), the H_2O concentrations of 1% partial melts of OIB source regions could range from 1·6 to 5·3 wt%. At 5% melting, these concentrations diminish to 0·5–1·7 wt% H_2O. Although these may be subordinate to CO_2 concentrations in the same melt, they may have a non-trivial influence on the locus of melting and on partial melt compositions.

Experiments detailing the effect of water on compositions of partial melts of peridotite have generally focused on hydrous magmatism in subduction zone settings (e.g. Gaetani & Grove, 1998; Falloon & Danyushevsky, 2000; Ulmer, 2001), and so there are few constraints on the influence of H_2O on the compositions of partial melts of garnet peridotite at fluid-undersaturated conditions. Hydrous melts with up to 12 wt% H_2O in equilibrium with garnet and spinel peridotite residua at 1·2–2 GPa show that H_2O promotes partial melts with high SiO_2 and low CaO/Al_2O_3 (Gaetani & Grove, 1998). Thus, the effect of H_2O on melt compositions may be the opposite to that required to explain highly alkalic magmas. However, modest concentrations of H_2O in a carbonated magma may compensate for some of the compositional effects of CO_2 that might otherwise be too extreme, such as high CaO/Al_2O_3. On the other hand, the hydrous, fluid-saturated peridotite melting experiments of Kawamoto & Holloway (1997) at 5–11 GPa produced ultramafic low-SiO_2 partial melts with very high CaO/Al_2O_3. Contrary to lower pressure results at less extreme H_2O concentrations, this may suggest that H_2O could enhance the alkalic characteristics of OIB at high pressure, but the relationship of these very hydrous ($\sim$50 wt% H_2O), highly magnesian (>25 wt% MgO) melts to OIB petrogenesis is unclear. Further experiments on partial melting of garnet lherzolite under water-undersaturated conditions and in the presence of mixed C–O–H volatiles are required to constrain the relative importance of CO_2 and H_2O in petrogenesis of alkalic OIB.

Geodynamic and geochemical considerations regarding the generation of alkalic silicate melts from partial melting of carbonated peridotite

Silicate partial melts derived from carbonated peridotite can have a number of compositional characteristics similar to alkalic OIB, but determining whether such melts contribute to OIB petrogenesis also requires consideration of the geodynamic conditions that may allow such partial melts to form beneath oceanic islands and the geochemical processes that may introduce appreciable carbon to the sources of alkalic OIB.

We infer that carbonated silicate melts plausibly parental to alkalic OIB may be produced at small degrees (1–5%) of partial melting from garnet peridotite with 0·1–0·25 wt% CO_2. Such melts may form at $1400 \pm 50^{\circ}C$ at 3 GPa (Dasgupta *et al.*, 2007), conditions that could be encountered along a normal ridge geotherm or the colder periphery of mantle plumes at about 90 km depth (Figs 15 and 16). On the other hand, similarly small-degree partial melts of these bulk compositions will occur at pressures up to 5 GPa, or depths of $\sim$150 km along higher temperature plume geotherms (Figs 15 and 16). An important question is whether such partial melts will be similar to alkalic OIB. Higher pressure partial melts may be enriched in FeO*, as is the case for partial melts of volatile-poor garnet peridotite (Walter, 1998) and this may help explain the remarkable FeO* enrichments in many alkalic OIB (Fig. 12). On the other hand, experiments in simple systems (Gudfinnsson & Presnall, 2005) indicate that partial melts of carbonated peridotite at pressures greater than 5 GPa become highly enriched in MgO and more akin to kimberlites rather than melilitites or nephelinites. High-pressure experiments with natural garnet peridotite and small amounts of bulk CO_2 are required to examine this question further.

Another crucial question is how carbon may become available to react with peridotite at appropriate temperature–pressure conditions to induce small-degree carbonated silicate partial melts. Upwelling solid carbonated peridotite will encounter its solidus at depths near 300 km for normal (sub-ridge) mantle potential temperatures and at depths approaching 400 km for hotter plume potential temperatures (Dasgupta & Hirschmann, 2006; Figs 15 and 16). However, the partial melt generated under these conditions is carbonatitic (Dasgupta & Hirschmann, 2006, 2007*a*, 2007*b*); carbonated silicate melting will occur at depths much shallower than the carbonated peridotite solidus along any plausible ridge or plume geotherm (Fig. 16). However, if the carbonatite partial melt that is formed at the carbonated peridotite solidus is extracted via porous flow, the residual peridotite will be virtually CO_2-free. Therefore, carbonated silicate partial melting of the peridotite at shallower depths requires a mechanism to bring carbon into contact with peridotite at conditions well above the solidus of carbonated peridotite.

One alternative is if the upwelling mantle is sufficiently reduced such that the carbon is in the form of diamond rather than magnesite. In this case, melting will occur shallower than the carbonated peridotite solidus and will

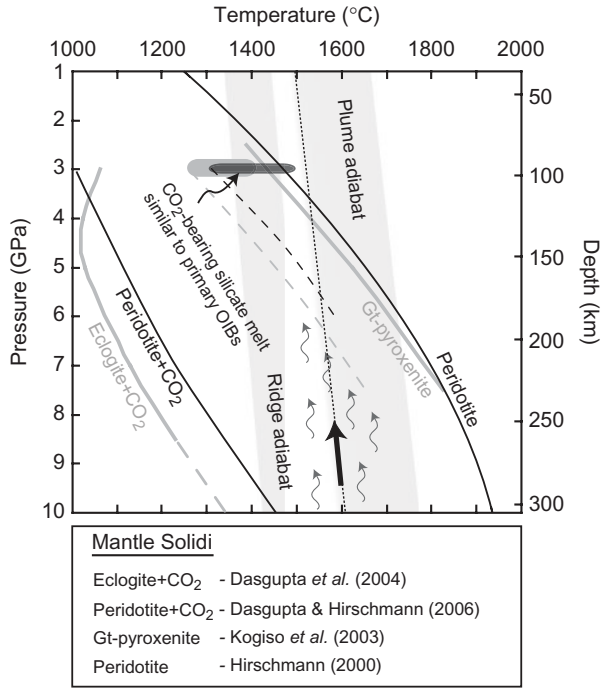

Fig. 15. Pressure–temperature diagram showing locations of various mantle solidi compared with the conditions of generation of carbonated silicate melts possibly similar to primary alkali ocean island basalts in equilibrium with peridotite (this study). Intersection between oceanic geotherms and carbonated mantle peridotite (Dasgupta & Hirschmann, 2006) and eclogite (Dasgupta *et al.*, 2004) solidi at very deep upper mantle conditions indicates likely generation of incipient carbonatitic melt at great depths. Reaction between buoyant carbonatitic melts (curved arrows) and overlying mantle peridotite will give rise to carbonated silicate melts at depths much shallower than carbonated mantle solidi, but significantly deeper than the solidus of volatile-free peridotite (Hirschmann, 2000). The P–T slopes of carbonated silicate melting for eclogite and peridotite are not experimentally constrained and so are plotted as dashed lines (grey for eclogite; black for peridotite) subparallel to the solidi of garnet pyroxenite (Kogiso *et al.*, 2003) and peridotite (Hirschmann, 2000), respectively.

commence at depths that depend on the redox state of the peridotite, producing carbonatite partial melts if the redox melting reaction occurs deeper or carbonated silicate partial melts if it occurs shallower. If the latter is the case, upwelling mantle peridotite may produce carbonated silicate melts by redox melting at depths just below the CO_2-free lherzolite solidus.

If carbon is released from upwelling lherzolite at depth as a carbonatite melt and this melt percolates upwards, it will ascend to depths where it may react with the surrounding mantle to produce carbonated silicate melts. In this case, the proportion of CO_2 that reacts with a given mass of peridotite depends not on the concentration of carbon in the mantle, but rather on the style of melt transport. If the ascending carbonatite melts rise via pervasive porous flow, such melting may be widespread and produce very low-degree carbonated silicate melts. On the other hand, if the carbonatite migrates in channels, then melting may be spatially restricted but locally much more extensive. Consequently, carbonated silicate partial melts with relatively high proportions of CO_2 may be produced even from ascending mantle for which the average CO_2 concentration may be low.

Possible role of pyroxenite and carbonated eclogite

Previously, it has been argued that many of the major element characteristics of alkalic OIB are potentially explained by contributions from partial melts of garnet pyroxenite (Hirschmann *et al.*, 2003; Kogiso *et al.*, 2003; Kogiso & Hirschmann, 2006) or carbonated eclogite (Dasgupta *et al.*, 2006). Whether the petrology of these lavas requires exotic lithologies in their source has been difficult to resolve owing in part to a dearth of direct experimental studies on partial melting of carbonated peridotite. The present study makes significant strides in providing such data. Partial melts of carbonated peridotite with 1 and 2·5 wt% CO_2 at 3 GPa have similarities to natural melilititic, nephelinitic, and basanitic OIB, and we believe that partial melts of peridotite with smaller amounts of CO_2 may yield liquids potentially parental to such lavas. Further development of the hypothesis attributing alkalic OIB to partial melting of carbonated peridotite will require more challenging experiments at lower melt fraction and with smaller amounts of bulk CO_2. Some of the features of nephelinites and melilitites, such as very high FeO^* and TiO_2, may not be reproduced by such partial melts, at least at 3 GPa and from normal composition peridotite. Partial melts of pyroxenite lithologies, or of peridotite that has been metasomatized by partial melts of pyroxenite, may be required.

Carbonated eclogite melts at depths even greater than that of carbonated peridotite (Dasgupta *et al.*, 2004) and produces carbonated silicate melts at temperatures lower than carbonated peridotite (Dasgupta *et al.*, 2006) (Figs 15 and 16). Dasgupta *et al.* (2006) noted that these carbonated silicate partial melts have extreme compositions that have many of the features of highly alkalic OIB, including low SiO_2 and low Al_2O_3, and high CaO, FeO^* and TiO_2. Dasgupta *et al.* (2006) considered several scenarios similar to that depicted in Fig. 16, in which such partial melts may contribute to the petrogenesis of alkalic OIB, including metasomatism leading to a TiO_2- and FeO^*-enriched carbonated peridotite with implanted trace element and isotopic signatures of crustal recycling. Such a scenario may allow for formation of alkalic OIB over a wider range of pressures and melt fractions than would otherwise be possible from unmetasomatized peridotite.

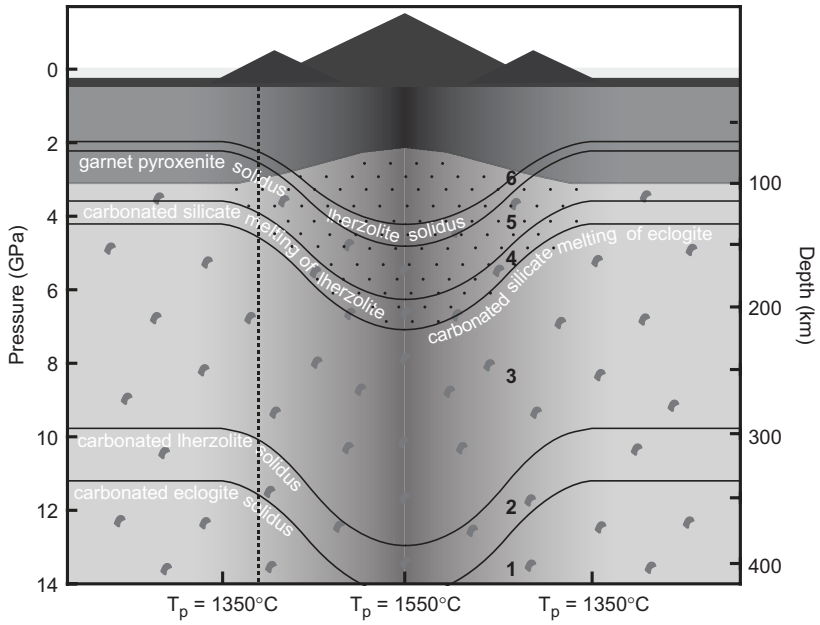

Fig. 16. Model of melting and metasomatism of a heterogeneous carbonated mantle in a thermally zoned axisymmetric mantle plume (e.g. Steinberger & Antretter, 2006). This diagram is based on the model presented by Dasgupta *et al.* (2006), but here the depths of carbonated silicate melting are quantified and the influence of temperature zonation of the plume is considered. The potential temperature (T_p) for the ambient mantle is assumed to be 1350°C (e.g. McKenzie *et al.*, 2005; Putirka, 2005; Herzberg *et al.*, 2007) and the plume axis to be 200°C hotter (Putirka, 2005; Herzberg *et al.*, 2007) with a non-linear temperature distribution across the plume (e.g. Steinberger & Antretter, 2006; a darker shade of grey implies higher temperature). In the region marked 'zone 1' in the figure, which occurs at depths greater than 340 km (plume periphery) to 410 km (plume core), CO_2 may be stored in peridotite and in eclogite or pyroxenite bodies (grey blobs), if the latter are present. Above the solidus of carbonated eclogite (zone 2; Dasgupta *et al.*, 2004), highly mobile carbonatite melts generated from eclogite are likely to migrate into surrounding peridotite, where they will solidify as metasomatic magnesite and clinopyroxene at the expense of orthopyroxene. Thus, in zone 2, regions of peridotite may be carbonated, either owing to a pre-existing carbonaceous component present at depth or owing to metasomatism by carbonatitic fluids derived from proximal eclogite bodies. Once the carbonated peridotite solidus (300–370 km deep: Dasgupta & Hirschmann, 2006) is crossed (zone 3), carbonatite melts may migrate freely through peridotite and eclogite. In zone 4, at depths shallower than 220–130 km, migrating carbonatite liquids that encounter eclogite bodies will react to form carbonated silicate melts. If such melts migrate into the surrounding peridotite, they will solidify, forming metasomatized peridotite enriched in FeO and TiO_2 (+ incompatible trace elements). Carbonated silicate melting can commence in peridotite in zone 5, beginning as deep as 110–200 km. In the absence of CO_2, partial melting of silica-deficient eclogite or garnet pyroxenite and peridotite will commence in zone 6. Delivery of unadulterated carbonated silicate melts to the lithosphere requires limited reaction with peridotite in zone 6 and above, and also limited or no contribution from partial melts of volatile-free peridotite; such conditions might be favoured at plume margins (e.g. vertical dashed line), where the volatile-free lherzolite solidus may not be intersected below the base of the lithosphere. Highly alkalic carbonated silicate partial melts of eclogite or peridotite are more likely to escape to the surface at the margins of the plume (or, alternatively, at the core of a plume that has a smaller excess potential temperature). Depths of melting of various lithologies are based on the intersection of solid mantle adiabats with mantle solidi as shown in Fig. 15 and the stippled zone marks the region of silicate melt production.

ACKNOWLEDGEMENTS

The authors are grateful for comments from John Longhi and Claude Herzberg, and for reviews by Fred Frey, James Tuff, Godfrey Fitton and an anonymous reviewer. Detailed comments by the journal editor Wendy Bohrson are also much appreciated. R.D. acknowledges support of Lamont–Doherty Earth Observatory of Columbia University for a post-doctoral fellowship during the preparation of the manuscript. This work received support from NSF grants EAR0310142 and EAR0609967.

REFERENCES

Albarède, F. (1992). How deep do common basaltic magmas form and differentiate? *Journal of Geophysical Research* **97**, 10997–11009.

Aubaud, C., Hauri, E. H. & Hirschmann, M. M. (2004). Hydrogen partition coefficients between nominally anhydrous minerals and basaltic melts. *Geophysical Research Letters* **31**, L20611, doi:10.1029/2004GL021341.

Aubaud, C., Pineau, F., Hékinian, R. & Javoy, M. (2005). Degassing of CO_2 and H_2O in submarine lavas from the Society hotspot. *Earth and Planetary Science Letters* **235**, 511–527.

Aubaud, C., Pineau, F., Hékinian, R. & Javoy, M. (2006). Carbon and hydrogen isotope constraints on degassing of CO_2 and H_2O in submarine lavas from the Pitcairn hotspot (South Pacific). *Geophysical Research Letters* **33**, L02308, doi:10.1029/2005GL024907.

Baker, M. B., Hirschmann, M. M., Ghiorso, M. S. & Stolper, E. M. (1995). Compositions of near-solidus peridotite melts from experiments and thermodynamic calculations. *Nature* **375**, 308–311, doi:10.1038/375308a0.

Blum, N., Halbach, P. & Münch, U. (1996). Geochemistry and mineralogy of alkali basalts from Tropic Seamount, Central Atlantic Ocean. *Marine Geology* **136**, 1–19.

Brey, G. (1978). Origin of olivine melilitites—chemical and experimental constraints. *Journal of Volcanology and Geothermal Research* **3**, 61–88.

Brey, G. & Green, D. H. (1975). The role of CO_2 in the genesis of olivine melilitite. *Contributions to Mineralogy and Petrology* **49**, 93–103.

Brey, G. P. & Green, D. H. (1976). Solubility of CO_2 in olivine melilitite at high pressures and role of CO_2 in Earth's mantle. *Contributions to Mineralogy and Petrology* **55**, 217–230.

Brey, G. & Green, D. H. (1977). Systematic study of liquidus phase relations in olivine melilitite + H_2O + CO_2 at high pressures and petrogenesis of an olivine melilitite magma. *Contributions to Mineralogy and Petrology* **61**, 141–162.

Brey, G. P., Kohler, T. & Nickel, K. G. (1990). Geothermometry in four-phase lherzolites I. Experimental results from 10 to 60 kb. *Journal of Petrology* **31**, 1313–1352.

Brooker, R. A., Kohn, S. C., Holloway, J. R. & McMillan, P. F. (2001). Structural controls on the solubility of CO_2 in silicate melts Part II: IR characteristics of carbonate groups in silicate glasses. *Chemical Geology* **174**, 241–254.

Bureau, H., Pineau, F., Métrich, N., Semet, M. P. & Javoy, M. (1998). A melt and fluid inclusion study of the gas phase at Piton de la Fournaise volcano (Réunion Island). *Chemical Geology* **147**, 115–130.

Canil, D. & O'Neill, H. S. C. (1996). Distribution of ferric iron in some upper mantle assemblages. *Journal of Petrology* **37**, 609–635.

Caroff, M., Maury, R. C., Guille, G. & Cotten, J. (1997). Partial melting below Tubuai (Austral Islands, French Polynesia). *Contributions to Mineralogy and Petrology* **127**, 369–382.

Clague, D. A. & Dalrymple, G. B. (1988). Age and petrology of alkalic postshield and rejuvenated-stage lava from Kauai, Hawaii. *Contributions to Mineralogy and Petrology* **99**, 202–218.

Clague, D. A. & Frey, F. A. (1982). Petrology and trace element geochemistry of the Honolulu volcanics, Oahu: Implications for the oceanic mantle below Hawaii. *Journal of Petrology* **23**, 447–504.

Dalton, J. A. & Presnall, D. C. (1998*a*). The continuum of primary carbonatitic–kimberlitic melt compositions in equilibrium with lherzolite: Data from the system CaO–MgO–Al_2O_3–SiO_2–CO_2 at 6 GPa. *Journal of Petrology* **39**, 1953–1964.

Dalton, J. A. & Presnall, D. C. (1998*b*). Carbonatitic melts along the solidus of model lherzolite in the system CaO–MgO–Al_2O_3–SiO_2–CO_2 from 3 to 7 GPa. *Contributions to Mineralogy and Petrology* **131**, 123–135.

Dalton, J. A. & Wood, B. J. (1993). The partitioning of Fe and Mg between olivine and carbonate and the stability of carbonate under mantle conditions. *Contributions to Mineralogy and Petrology* **114**, 501–509.

Dasgupta, R. & Hirschmann, M. M. (2006). Melting in the Earth's deep upper mantle caused by carbon dioxide. *Nature* **440**, 659–662.

Dasgupta, R. & Hirschmann, M. M. (2007*a*). Effect of variable carbonate concentration on the solidus of mantle peridotite. *American Mineralogist* **92**, 370–379.

Dasgupta, R. & Hirschmann, M. M. (2007*b*). A modified iterative sandwich method for determination of near-solidus partial melt compositions. II. Application to determination of near-solidus melt compositions of carbonated peridotite. *Contributions to Mineralogy and Petrology* [doi:10.1007/s00410-007-0214-8].

Dasgupta, R., Hirschmann, M. M. & Withers, A. C. (2004). Deep global cycling of carbon constrained by the solidus of anhydrous, carbonated eclogite under upper mantle conditions. *Earth and Planetary Science Letters* **227**, 73–85.

Dasgupta, R., Hirschmann, M. M. & Dellas, N. (2005). The effect of bulk composition on the solidus of carbonated eclogite from partial melting experiments at 3 GPa. *Contributions to Mineralogy and Petrology* **149**, 288–305.

Dasgupta, R., Hirschmann, M. M. & Stalker, K. (2006). Immiscible transition from carbonate-rich to silicate-rich melts in the 3 GPa melting interval of eclogite + CO_2 and genesis of silica-undersaturated ocean island lavas. *Journal of Petrology* **47**, 647–671.

Dasgupta, R., Hirschmann, M. M. & Smith, N. D. (2007). Water follows carbon: CO_2 incites deep silicate melting and dehydration beneath mid-ocean ridges. *Geology* **35**, 135–138, doi:110.1130/G22856A.22851.

Dixon, J. E. & Clague, D. A. (2001). Volatiles in basaltic glasses from Loihi seamount, Hawaii: evidence for a relatively dry plume component. *Journal of Petrology* **42**, 627–654.

Dixon, J. E., Clague, D. A., Wallace, P. & Poreda, R. (1997). Volatiles in alkalic basalts from the North Arch volcanic field, Hawaii: extensive degassing of deep submarine-erupted alkalic series lavas. *Journal of Petrology* **38**, 911–939.

Dixon, J. E., Leist, L., Langmuir, C. & Schilling, J.-G. (2002). Recycled dehydrated lithosphere observed in plume-influenced mid-ocean-ridge basalts. *Nature* **420**, 385–389.

Eggler, D. H. (1974). Effect of CO_2 on the melting of peridotite. *Carnegie Institution of Washington Yearbook* **73**, 215–224.

Eggler, D. H. (1978). The effect of CO_2 upon partial melting of peridotite in the system Na_2O–CaO–Al_2O_3–MgO–SiO_2–CO_2 to 35 kb, with an analysis of melting in a peridotite–H_2O–CO_2 system. *American Journal of Science* **278**, 305–343.

Falloon, T. J. & Danyushevsky, L. V. (2000). Melting of refractory mantle at 1·5, 2 and 2·5 GPa under anhydrous and H_2O-undersaturated conditions: Implications for the petrogenesis of high-Ca boninites and the influence of subduction components on mantle melting. *Journal of Petrology* **41**, 257–283.

Falloon, T. J. & Green, D. H. (1989). The solidus of carbonated, fertile peridotite. *Earth and Planetary Science Letters* **94**, 364–370.

Frey, F. A., Wise, W. S., Garcia, M. O., West, H., Kwon, S.-T. & Kennedy, A. (1990). Evolution of Mauna Kea Volcano, Hawaii: Petrologic and geochemical constraints on postshield volcanism. *Journal of Geophysical Research* **95**(B2), 1271–1300.

Frost, D. J. & Wood, B. J. (1997). Experimental measurements of the fugacity of CO_2 and graphite/diamond stability from 35 to 77 kbar at 925 to 1650°C. *Geochimica et Cosmochimica Acta* **61**, 1565–1574.

Gaetani, G. A. & Grove, T. L. (1998). The influence of water on melting of mantle peridotite. *Contributions to Mineralogy and Petrology* **131**, 323–346.

Garcia, M. O., Foss, D. J. P., West, H. B. & Mahoney, J. (1995). Geochemical and isotopic evolution of Loihi volcano, Hawaii. *Journal of Petrology* **36**, 1647–1674.

Gee, L. L. & Sack, R. O. (1988). Experimental petrology of melilite nephelinites. *Journal of Petrology* **29**, 1233–1255.

Green, D. H. (1973). Experimental melting studies on a model upper mantle composition at high pressure under water-saturated and water-undersaturated conditions. *Earth and Planetary Science Letters* **19**, 37–53.

Green, D. H. & Falloon, T. J. (1998). Pyrolite: A Ringwood concept and its current expression. In: Jackson, I. (ed.) *The Earth's Mantle: Composition, Structure, and Evolution*. Cambridge: Cambridge University Press, pp. 311–378.

Green, D. H. & Ringwood, A. E. (1967). The genesis of basaltic magmas. *Contributions to Mineralogy and Petrology* **15**, 103–190.

Gudfinnsson, G. & Presnall, D. C. (2005). Continuous gradations among primary carbonatitic, kimberlitic, melilititic, basaltic, picritic, and komatiitic melts in equilibrium with garnet lherzolite at 3–8 GPa. *Journal of Petrology* **46**, 1645–1659.

Gudmundsson, G. & Wood, B. J. (1995). Experimental tests of garnet peridotite oxygen barometry. *Contributions to Mineralogy and Petrology* **119**, 56–67.

Hauri, E. H., Gaetani, G. A. & Green, T. H. (2006). Partitioning of water during melting of the Earth's upper mantle at H_2O-undersaturated conditions. *Earth and Planetary Science Letters* **248**, 715–734.

Hémond, C., Devey, C. W. & Chauvel, C. (1994). Source compositions and melting processes in the Society and Austral plumes (South Pacific Ocean): Element and isotope (Sr, Nd, Pb, Th) geochemistry. *Chemical Geology* **115**, 7–45.

Herzberg, C. & O'Hara, M. J. (2002). Plume-associated ultramafic magmas of Phanerozoic age. *Journal of Petrology* **43**, 1857–1883.

Herzberg, C., Raterron, P. & Zhang, J. (2000). New experimental observations on the anhydrous solidus for peridotite KLB-1. *Geochemistry, Geophysics, Geosystems* **1**, paper number 2000GC000089.

Herzberg, C., Asimow, P. D., Arndt, N., Niu, Y., Lesher, C. M., Fitton, J. G., Cheadle, M. J. & Saunders, A. D. (2007). Temperatures in ambient mantle and plumes: Constraints from basalts, picrites, and komatiites. *Geochemistry, Geophysics, Geosystems* **8**, Q02006, doi:02010.01029/02006GC001390.

Hirano, N., Takahashi, E., Yamamoto, J., Abe, N., Ingle, S. P., Kaneoka, I., Hirata, T., Kimura, J.-I., Ishii, T., Ogawa, Y., Machida, S. & Suyehiro, K. (2006). Volcanism in response to plate flexure. *Science* **313**, 1426–1428.

Hirose, K. (1997). Partial melt compositions of carbonated peridotite at 3 GPa and role of CO_2 in alkali-basalt magma generation. *Geophysical Research Letters* **24**, 2837–2840.

Hirose, K. & Kushiro, I. (1993). Partial melting of dry peridotites at high pressures: Determination of compositions of melts segregated from peridotite using aggregates of diamond. *Earth and Planetary Science Letters* **114**, 477–489.

Hirschmann, M. M. (2000). The mantle solidus: experimental constraints and the effect of peridotite composition. *Geochemistry, Geophysics, Geosystems* **1**, paper number 2000GC000070.

Hirschmann, M. M., Baker, M. B. & Stolper, E. M. (1998). The effect of alkalis on the silica content of mantle derived melts. *Geochimica et Cosmochimica Acta* **62**, 883–902.

Hirschmann, M. M., Ghiorso, M. S. & Stolper, E. M. (1999). Calculation of peridotite partial melting from thermodynamic models of minerals and melts. II. Isobaric variations in melts near the solidus and owing to variable source composition. *Journal of Petrology* **40**, 297–313.

Hirschmann, M. M., Kogiso, T., Baker, M. B. & Stolper, E. M. (2003). Alkalic magmas generated by partial melting of garnet pyroxenite. *Geology* **31**, 481–484.

Hirth, G. & Kohlstedt, D. L. (1996). Water in the oceanic upper mantle: implications for rheology, melt extraction, and the evolution of the lithosphere. *Earth and Planetary Science Letters* **144**, 93–108.

Hoernle, K., Tilton, G., Le Bas, M. J., Duggen, S. & Schönberg, D. G. (2002). Geochemistry of oceanic carbonatites compared with continental carbonatites: mantle recycling of oceanic crustal carbonate. *Contributions to Mineralogy and Petrology* **142**, 520–542.

Hofmann, A. W. (1997). Mantle geochemistry: the message from oceanic volcanism. *Nature* **385**, 219–229.

Holm, P. M., Wilson, J. R., Christensen, B. P., Hansen, L., Hansen, S. L., Hein, K. M., Mortensen, A. K., Pedersen, R., Plesner, S. & Runge, M. K. (2006). Sampling the Cape Verde mantle plume: evolution of melt compositions on Santo Antão, Cape Verde Islands. *Journal of Petrology* **47**, 145–189.

Ito, G. & Mahoney, J. J. (2005*a*). Flow and melting of a heterogeneous mantle: 1. Method and importance to the geochemistry of ocean island and mid-ocean ridge basalts. *Earth and Planetary Science Letters* **230**, 29–46.

Ito, G. & Mahoney, J. J. (2005*b*). Flow and melting of a heterogeneous mantle: 2. Implications for a chemically nonlayered mantle. *Earth and Planetary Science Letters* **230**, 47–63.

Ito, K. & Kennedy, G. C. (1967). Melting and phase relations in a natural peridotite to 40 kbar. *American Journal of Science* **265**, 519–538.

Janney, P. E., Macdougall, J. D., Natland, J. H. & Lynch, M. A. (2000). Geochemical evidence from the Pukapuka volcanic ridge system for a shallow enriched mantle domain beneath the South Pacific Superswell. *Earth and Planetary Science Letters* **181**, 47–60.

Javoy, M. & Pineau, F. (1991). The volatiles record of a 'popping' rock from the Mid-Atlantic Ridge at 14°N: chemical and isotopic composition of gas trapped in the vesicles. *Earth and Planetary Science Letters* **107**, 598–611.

Kamenetsky, V. S., Everard, J. L., Crawford, A. J., Varne, R., Eggins, S. M. & Lanyon, R. (2000). Enriched end-member of primitive MORB melts: petrology and geochemistry of glasses from Macquarie Island (SW Pacific). *Journal of Petrology* **41**, 411–430.

Kawamoto, T. & Holloway, J. R. (1997). Melting temperature and partial melt chemistry of H_2O-saturated mantle peridotite to 11 gigapascals. *Science* **276**, 240–243.

Kogiso, T. & Hirschmann, M. M. (2006). Partial melting experiments of bimineralic eclogite and the role of recycled mafic oceanic crust in the genesis of ocean island basalts. *Earth and Planetary Science Letters* **249**, 188–199.

Kogiso, T., Hirose, K. & Takahashi, E. (1998). Melting experiments on homogeneous mixtures of peridotite and basalt: application to the genesis of ocean island basalts. *Earth and Planetary Science Letters* **162**, 45–61.

Kogiso, T., Hirschmann, M. M. & Frost, D. J. (2003). High-pressure partial melting of garnet pyroxenite: possible mafic lithologies in the source of ocean island basalts. *Earth and Planetary Science Letters* **216**, 603–617.

Korenaga, J. (2005). Why did not the Ontong Java Plateau form subaerially? *Earth and Planetary Science Letters* **234**, 385–399.

Kushiro, I. (1975). On the nature of silicate melt and its significance in magma genesis: regularities in the shift of the liquidus boundaries involving olivine, pyroxene, and silica minerals. *American Journal of Science* **275**, 411–431.

Kushiro, I. (1996). Partial melting of a fertile mantle peridotite at high pressures: An experimental study using aggregates of diamond. In: Basu, A. & Hart, S. (eds) *Earth Processes: Reading the Isotopic Code. Geophysical Monograph, American Geophysical Union* **95**, 109–122.

Kushiro, I. (2001). Partial melting experiments on peridotite and origin of mid-ocean ridge basalt. *Annual Review of Earth and Planetary Sciences* **29**, 71–107.

Kushiro, I. & Mysen, B. O. (2002). A possible effect of melt structure on the $Mg–Fe^{2+}$ partitioning between olivine and melt. *Geochimica et Cosmochimica Acta* **66**, 2267–2272.

Kushiro, I. & Walter, M. J. (1998). Mg–Fe partitioning between olivine and mafic–ultramafic melts. *Geophysical Research Letters* **25**, 2337–2340.

Langmuir, C. H., Klein, E. M. & Plank, T. (1992). Petrological systematics of mid-ocean ridge basalts: constraints on melt generation beneath ocean ridges. In: Phipps Morgan, J., Blackman, D. K. & Sinton, J. M. (eds) *Mantle Flow and Melt Generation at Mid-ocean Ridges. Geophysical Monograph, American Geophysical Union* **71**, 183–280.

Lassiter, J. C., DePaolo, D. J. & Tatsumoto, M. (1996). Isotopic evolution of Mauna Kea volcano: Results from the initial phase of the Hawiian Scientific Drilling Project. *Journal of Geophysical Research* **101**, 11769–11780.

LeBas, M. J. (1989). Nephelinitic and basanitic rocks. *Journal of Petrology* **30**, 1299–1312.

Lee, W.-J. & Wyllie, P. J. (1997). Liquid immiscibility between nephelinite and carbonatite from 1·0 to 2·5 GPa compared with mantle melt compositions. *Contributions to Mineralogy and Petrology* **127**, 1–16.

Longhi, J., Walker, D. & Hays, J. F. (1978). The distribution of Fe and Mg between olivine and lunar basaltic liquids. *Geochimica et Cosmochimica Acta* **42**, 1545–1558.

Maaløe, S., James, D., Smedley, P., Petersen, S. & Garmann, L. B. (1992). The Kola volcanic suite of Kauai, Hawaii. *Journal of Petrology* **33**, 761–784.

McDonough, W. F. & Sun, S.-s. (1995). The composition of the Earth. *Chemical Geology* **120**, 223–253.

McKenzie, D., Jackson, J. & Priestley, K. (2005). Thermal structure of oceanic and continental lithosphere. *Earth and Planetary Science Letters* **233**, 337–349.

Meibom, A. & Anderson, D. L. (2004). The statistical upper mantle assemblage. *Earth and Planetary Science Letters* **217**, 123–139.

Moore, K. R. & Wood, B. J. (1998). The transition from carbonate to silicate melts in the CaO–MgO–SiO_2–CO_2 system. *Journal of Petrology* **39**, 1943–1951.

Morgan, J. P. & Morgan, W. J. (1999). Two-stage melting and the geochemical evolution of the mantle: a recipe for mantle plum-pudding. *Earth and Planetary Science Letters* **170**, 215–239.

Morgan, W. J. (1971). Convective plumes in the lower mantle. *Nature* **230**, 42–43.

Mysen, B. O. & Boettcher, A. L. (1975). Melting of a hydrous mantle: I. Phase relations of natural peridotite at high pressures and temperatures with controlled activities of water, carbon dioxide, and hydrogen. *Journal of Petrology* **16**, 520–548.

Neumann, E.-R., Wulff-Pedersen, E., Pearson, N. J. & Spencer, E. A. (2002). Mantle xenoliths from Tenerife (Canary Islands): evidence for reactions between mantle peridotites and silicic carbonatite melts inducing Ca metasomatism. *Journal of Petrology* **43**, 825–857.

Nichols, A. R. L., Carroll, M. R. & Höskuldsson, Á. (2002). Is the Iceland hotspot also wet? Evidence from the water contents of undegassed submarine and subglacial pillow basalts. *Earth and Planetary Science Letters* **202**, 77–87.

Norman, M. D., Garcia, M. O., Kamenetsky, V. S. & Nielsen, R. L. (2002). Olivine-hosted melt inclusions in Hawaiian picrites: equilibration, melting, and plume source characteristics. *Chemical Geology* **183**, 143–168.

Olafsson, M. & Eggler, D. H. (1983). Phase relations of amphibole, amphibole–carbonate, and phlogopite–carbonate peridotite: petrologic constraints on the asthenosphere. *Earth and Planetary Science Letters* **64**, 305–315.

Pineau, F., Shilobreeva, S., Hekinian, R., Bidiau, D. & Javoy, M. (2004). Deep-sea explosive activity on the Mid-Atlantic Ridge near 34°50′N: a stable isotope (C, H, O) study. *Chemical Geology* **118**, 43–64.

Presnall, D. C., Gudfinnsson, G. H. & Walter, M. J. (2002). Generation of mid-ocean ridge basalts at pressures from 1 to 7 GPa. *Geochimica et Cosmochimica Acta* **66**, 2073–2090.

Putirka, K. D. (2005). Mantle potential temperatures at Hawaii, Iceland, and the mid-ocean ridge system, as inferred from olivine phenocrysts: evidence for thermally driven mantle plumes. *Geochemistry, Geophysics, Geosystems* **6**, Q05L08, doi:10.1029/2005GC000915.

Raddick, M. J., Parmentier, E. M. & Scheirer, D. S. (2002). Buoyant decompression melting: A possible mechanism for intraplate volcanism. *Journal of Geophysical Research* **107**, (B10), 2228, doi:2210.1029/2001JB000617.

Ren, Z.-Y., Shibata, T., Yoshkawa, M., Johnson, K. T. M. & Takahashi, E. (2006). Isotope compositions of submarine Hana Ridge lavas, Haleakala volcano, Hawaii: implications for source compositions, melting process and the structure of the Hawaiian plume. *Journal of Petrology* **47**, 255–275.

Roeder, P. L. & Emslie, R. F. (1970). Olivine–liquid equilibrium. *Contributions to Mineralogy and Petrology* **29**, 275–289.

Ryabchikov, I. D., Brey, G., Kogarko, L. N. & Bulatov, V. K. (1989). Partial melting of carbonatized peridotite at 50 kbar. *Geokhimiya* **1**, 3–9.

Saal, A. E., Hart, S. R., Shimizu, N., Hauri, E. H. & Layne, G. D. (1998). Pb isotopic variability in melt inclusions from oceanic island basalts, Polynesia. *Science* **282**, 1481–1484.

Seaman, C., Sherman, S. B., Garcia, M. O., Baker, M. B., Balta, B. & Stolper, E. (2004). Volatiles in glasses from the HSDP2 drill core. *Geochemistry, Geophysics, Geosystems* **5**, Q09G16, doi:10.1029/2003GC000596.

Sobolev, A. V., Hofmann, A. W., Sobolev, S. V. & Nikogosian, I. K. (2005). An olivine-free mantle source of Hawaiian shield basalts. *Nature* **434**, 590–597.

Steinberger, B. & Antretter, M. (2006). Conduit diameter and buoyant rising speed of mantle plumes: Implications for the motion of hot spots and shape of plume conduits. *Geochemistry, Geophysics, Geosystems* **7**, Q11018, doi:11010.11029/12006GC001409.

Tackley, P. J. (2000). Mantle convection and plate tectonics: toward an integrated physical and chemical theory. *Science* **288**, 2002–2007.

Takahashi, E. (1986). Melting of a dry peridotite KLB-1 up to 14 GPa: Implications on the origin of peridotitic upper mantle. *Journal of Geophysical Research* **91**, 9367–9382.

Takahashi, E. & Kushiro, I. (1983). Melting of a dry peridotite at high pressures and basalt magma genesis. *American Mineralogist* **68**, 859–879.

Toplis, M. J. (2005). The thermodynamics of iron and magnesium partitioning between olivine and liquid: criteria for assessing and predicting equilibrium in natural and experimental systems. *Contributions to Mineralogy and Petrology* **149**, 22–39, doi:10.1007/s00410-00004-00629-00414.

Ulmer, P. (1989). The dependence of the Fe^{2+}–Mg cation partitioning between olivine and basaltic liquid on pressure, temperature and composition. *Contributions to Mineralogy and Petrology* **101**, 261–270.

Ulmer, P. (2001). Partial melting in the mantle wedge—the role of H_2O in the genesis of mantle-derived 'arc-related' magmas. *Physics of the Earth and Planetary Interiors* **127**, 215–232.

Wagner, T. P. & Grove, T. L. (1998). Melt/harzburgite reaction in the petrogenesis of tholeiitic magma from Kilauea volcano, Hawaii. *Contributions to Mineralogy and Petrology* **131**, 1–12.

Walter, M. J. (1998). Melting of garnet peridotite and the origin of komatiite and depleted lithosphere. *Journal of Petrology* **39**, 29–60.

Walter, M. J., Sisson, T. W. & Presnall, D. C. (1995). A mass proportion method for calculating melting reactions and application to melting of model upper mantle lherzolite. *Earth and Planetary Science Letters* **135**, 77–90.

Wendlandt, R. F. & Mysen, B. O. (1980). Melting phase relations of natural peridotite + CO_2 as a function of degree of partial melting at 15 and 30 kbar. *American Mineralogist* **65**, 37–44.

West, H. B., Garcia, M. O., Frey, F. A. & Kennedy, A. (1988). Nature and cause of compositional variation among the alkalic cap lavas of Mauna Kea Volcano, Hawaii. *Contributions to Mineralogy and Petrology* **100**, 383–397.

Workman, R. K. & Hart, S. R. (2005). Major and trace element composition of the depleted MORB mantle (DMM). *Earth and Planetary Science Letters* **231**, 53–72.

Wyllie, P. J. (1979). Magmas and volatile components. *American Mineralogist* **64**, 469–500.

Wyllie, P. J. & Huang, W.-L. (1976). Carbonation and melting reactions in the system $CaO–MgO–SiO_2–CO_2$ at mantle pressures with geophysical and petrological applications. *Contributions to Mineralogy and Petrology* **54**, 79–107.

Xirouchakis, D., Hirschmann, M. M. & Simpson, J. A. (2001). The effect of titanium on the silica content and on mineral–liquid partitioning of mantle-equilibrated melts. *Geochimica et Cosmochimica Acta* **65**, 2201–2217.

Yang, H.-J., Frey, F. A. & Clague, D. A. (2003). Constraints on the source components of lavas forming the Hawaiian North Arch and Honolulu volcanics. *Journal of Petrology* **44**, 603–627 .